PHYSICAL REVIEW A **88**, 033410 (2013)

Zero-range-potential model for strong-field molecular processes: Dynamic polarizability and photodetachment cross section

S. V. Borzunov,[1] M. V. Frolov,[2] M. Yu. Ivanov,[2,3] N. L. Manakov,[2] S. S. Marmo,[2] and Anthony F. Starace[4]

[1]*Department of Computer Science, Voronezh State University, Voronezh 394006, Russia*

[2]*Department of Physics, Voronezh State University, Voronezh 394006, Russia*

[3]*Max-Born Institute, Max-Born-Strasse 2A, Berlin D-12489, Germany*

[4]*Department of Physics and Astronomy, The University of Nebraska, Lincoln, Nebraska 68588-0299, USA*

(Received 4 July 2013; published 9 September 2013)

We develop a general theoretical framework for the analytical description of the interaction of a model diatomic molecular system with an intense, arbitrarily polarized monochromatic laser field. The model molecule comprises an electron in the field of two zero-range potentials separated by the internuclear distance. This model has an exact analytical solution within the theoretical framework of the quasistationary quasienergy (Floquet) approach. In addition to the development of this general framework, we also present a detailed analysis of the weak-field limit, within which we obtain both the frequency-dependent polarizability and the angle-resolved photodetachment cross section for the model system. These fundamental properties are analyzed for both homonuclear and heteronuclear molecular systems in a linearly polarized laser field, for both ground and excited electronic states, and for arbitrary orientation of the molecular axis relative to the polarization vector of the laser field. The analytical expressions for the polarizability and angle-resolved photoelectron spectra exhibit characteristic double-slit interference patterns, allowing one to study their dependence on the parameters of the problem beyond the level of the Born approximation.

DOI: 10.1103/PhysRevA.88.033410 PACS number(s): 33.80.Eh, 33.20.Xx

I. INTRODUCTION

The interaction of intense laser fields with diatomic molecules provides a wider range of strong-field phenomena than is the case for intense laser interactions with atoms. This wider range of phenomena stems from the additional nucleus, which can bind an electron or from which an electron can scatter. Additionally, it introduces an additional parameter of the problem, the internuclear separation vector, **R**, between the two nuclei. Strong-field molecular processes depend significantly on both the magnitude of **R** and its direction relative to the laser polarization vector. Examples of molecular strong-field phenomena include above-threshold dissociation [1], molecular bond softening [2], electron-localization effects (as R increases) on molecular ionization [3–5], molecular alignment effects on ionization [6–9], molecular orbital symmetry effects on ionization rates [10], and laser polarization effects on molecular above-threshold ionization [11].

An increasingly active area of research is directed at obtaining information concerning target molecular properties from strong-field molecular spectra. For the strong-field process of high-order harmonic generation (HHG), the HHG spectrum of an aligned N_2 molecule was used to obtain a tomographic image of the highest occupied molecular orbital of N_2 [12]. This approach, however, assumes that the active (laser-driven) molecular electron may be described by a free electron rather than an electron moving in the field of the molecular ion. A more accurate theory, the quantitative rescattering (QRS) theory [13], assumes that the (frequency-domain) HHG spectrum of a molecule can be expressed as the product of a wave packet (representing the active laser-driven electron) and the field-free photorecombination cross section of the molecular ion, which can be obtained very accurately either by a separate calculation or from experimental data. (For a factorization in the time domain, see, e.g., Ref. [14].) Alternatively, the QRS theory may be used to obtain the field-free photorecombination cross section of a molecule from its strong-field HHG spectrum, assuming the electron wave packet can be calculated accurately. The QRS theory has also been used to analyze intense laser ionization of aligned molecules. For example, laser-induced rescattering photoelectron spectroscopy has been used to extract field-free electron-molecular ion elastic scattering differential cross sections [15]. It has also been employed in laser-induced electron diffraction (LIED) of aligned molecules to obtain not only field-free elastic differential cross sections but also information on molecular bond lengths [16]. (It should be noted that LIED investigations can be carried out not only using linearly polarized intense laser fields but also using circularly polarized laser fields [17], owing to the much greater spatial extent of a molecular target as compared to an atomic one.)

The connection between strong-field molecular processes and field-free molecular properties has been established empirically, based upon accurate quantum calculations of the field-free molecular properties and upon either numerical solutions of the time-dependent Schrödinger equation (TDSE) or strong-field approximation (SFA) calculations of the strong-field molecular processes (see, e.g., Ref. [13]). An analytic quantum proof of the factorization of a strong-field molecular process as the product of an electron wave-packet factor, dependent on laser parameters, and a field-free molecular property, independent of laser parameters, has yet to be given. While such an analytic proof for any real molecular system is unlikely, such a proof may prove possible for a simple model of a diatomic molecule.

This latter expectation is based upon our experience in successfully obtaining analytic derivations of such factorizations for many strong-field atomic processes based upon a simple model of an atom. In this model we assume that a single electron is bound in a short-range potential and interacts with

 ©2013 American Physical Society

a monochromatic laser field. The electron's interactions with both the short-range potential and the laser field are treated exactly and nonperturbatively. We have termed the theory for this model system the time-dependent effective range (TDER) theory [18,19]. Based on TDER theory, we have shown analytically [20,21] that HHG rates do indeed factorize into three factors, each corresponding to one of the three steps of the three-step scenario: a tunneling ionization factor, a factor describing the laser-driven motion of the electron in the laser field, and a factor describing the recombination of the electron to its ground state in the short-range potential with the emission of a harmonic photon. For each factor, a closed-form analytic expression was obtained. Since the factor describing electron motion in the laser field is independent of the atom, it is a universal factor appropriate for any atom. The tunneling factor and the photorecombination factor of course depend on the particular atom's parameters. However, the physical meaning of these factors is so transparent that real atoms can be described by simply replacing the model factors with factors appropriate for the real atom under consideration [22]. Using this simple model, analytic proofs of the factorization of other strong-field processes have been given, including above-threshold ionization (ATI) [23] and laser-assisted electron-atom scattering [24,25]. While the above analytic derivations have been given for strong-field processes involving monochromatic laser fields, analytic results have also been derived for both HHG [26,27] and ATI [28] by short, intense laser pulses. Furthermore, the analytical results have shown that factorization of the rates for strong-field processes in the frequency domain is not universal. For example, we have recently shown that for HHG driven by an intense laser field with a small elliptical polarization such factorization holds only for s electrons but not for p electrons [29], while for short-pulse ATI [28] and laser-assisted radiative recombination [30] the factorization does not hold in general even for a linearly polarized field.

In this paper we describe a simple model for a diatomic molecular ion interacting with an intense, monochromatic laser field. In this model the potential of each nuclear center is described by a zero-range (or δ function) potential (ZRP) and there is only a single electron. This model was introduced in Ref. [31] to simulate the electron dynamics in a two-center (molecular) system as the generalization of the well-known single center ZRP model. It is widely used for a range of molecular and collision problems (cf., e.g., the book [32] and references therein). To the best of our knowledge, this model was first used for the description of strong-field processes in Ref. [33] for the case of a static electric field (see also the recent paper [34]) and in Ref. [35] for the case of a circularly polarized field. In the latter paper, the results of Refs. [36,37] for the complex quasienergy of a weakly bound electron in a single ZRP model were generalized to the case of an electron in the field of two δ centers. An analysis of HHG for the ZRP model molecular ion system was given in Ref. [38], obtaining analytic expressions for HHG rates (up to one final quadrature) using the SFA within an S-matrix approach. However, in Ref. [38] the ZRP molecular model is used only on a "field-free" level, i.e., using the field-free wave function of the bound electron and employing the Volkov Green function for the description of its evolution in the laser field. Here we formulate the problem using a Floquet or quasistationary quasienergy state (QQES) approach. In addition to the general development of the QQES theory for the ZRP molecular model, applicable for the description of any strong-field process involving the molecular model, our goal in this paper is to analyze the weak-field limit of the general problem, thereby obtaining results for the dynamic polarizability and the differential photodetachment cross section of the molecular ion. As far as we are aware, photodetachment for this simple molecular ion system has been analyzed previously only within the plane-wave approximation [39–43], which we do not employ in our analysis. Obtaining analytic expressions for the photodetachment cross section of this simple molecular ion model is the first step towards the goal of determining whether the strong-field HHG rates for this model system factorize into laser-dependent and field-free (photorecombination) factors.

The paper is organized as follows. In Sec. II we present some basic results for the field-free molecular model that are necessary to generalize this model to the case of a model molecular system interacting with a strong monochromatic field. This generalization in the framework of the QQES approach is presented in Sec. III, in which we derive the general equations for the QQES wave function and the complex quasienergy, as well as for the differential probability of n-photon detachment in a strong elliptically polarized field. The weak-field limits of the general results in Sec. III are analyzed in Secs. IV and V, in which explicit analytic results for the dynamic polarizability and the differential cross section for one-photon detachment are obtained in the lowest order of perturbation theory (PT) for the particular case of a linearly polarized laser field. Numerical results are presented and discussed in Sec. VI. The main results of the paper are summarized in Sec. VII. Two Appendices contain some technical details of the calculations.

Atomic units are used through the paper.

II. FIELD-FREE MOLECULAR MODEL

Within the ZRP molecular model, the bound-state wave function, $\psi_E(\mathbf{r})$, of an electron in the field of two (generally not identical) attractive atomic centers, separated by the distance $R = |\mathbf{R}| = |\mathbf{R}_1 - \mathbf{R}_2|$ and localized at positions $\mathbf{R}_1 = \mathbf{R}/2$ and $\mathbf{R}_2 = -\mathbf{R}/2$, is represented as a linear combination of one-center ZRP-like wave functions located at each of two centers [32]:

$$\psi_E(\mathbf{r}) = \psi_E^{(1)}(\mathbf{r}) + \psi_E^{(2)}(\mathbf{r}) = c_1 \frac{e^{-\sqrt{-2E}|\mathbf{r}-\mathbf{R}_1|}}{|\mathbf{r}-\mathbf{R}_1|} + c_2 \frac{e^{-\sqrt{-2E}|\mathbf{r}-\mathbf{R}_2|}}{|\mathbf{r}-\mathbf{R}_2|}. \quad (1)$$

The main advantage of the molecular ZRP model is that, similarly to the case of a one-center δ potential, the wave function $\psi_E(\mathbf{r})$ satisfies prescribed boundary conditions at the position of each δ center [32],

$$\psi_E(\mathbf{r})|_{\mathbf{r}\to\mathbf{R}_j} \approx c_j \left(\frac{1}{|\mathbf{r}-\mathbf{R}_j|} - \kappa_j \right), \quad j = 1,2, \quad (2)$$

where the positive parameter κ_j determines the energy, $E_j^{(0)} = -\kappa_j^2/2$, of a single bound s state supported by an isolated jth δ center. (Note also that κ_j^{-1} is the scattering length

for electron scattering by the jth center; for definiteness, we assume $\kappa_1 \geqslant \kappa_2$.)

Matching the wave function (1) to the boundary conditions (2), we obtain a system of two homogeneous linear equations for the coefficients c_1 and c_2,

$$\begin{pmatrix} \kappa_1 - \sqrt{-2E} & \frac{e^{-\sqrt{-2E}R}}{R} \\ \frac{e^{-\sqrt{-2E}R}}{R} & \kappa_2 - \sqrt{-2E} \end{pmatrix} \begin{pmatrix} c_1 \\ c_2 \end{pmatrix} = 0, \tag{3}$$

while the energy E is given by the roots of the determinant of the 2×2 matrix in Eq. (3):

$$(\kappa_1 - \sqrt{-2E})(\kappa_2 - \sqrt{-2E}) - \frac{e^{-2\sqrt{-2E}R}}{R^2} = 0. \tag{4}$$

Equation (4) can be split into two independent equations:

$$\sqrt{-2E_\pm} - \kappa_+ = \pm\sqrt{\kappa_-^2 + \frac{e^{-2\sqrt{-2E_\pm}R}}{R^2}}, \tag{5}$$

where $\kappa_+ = (\kappa_1 + \kappa_2)/2$ and $\kappa_- = (\kappa_1 - \kappa_2)/2$.

We parametrize the energies $E_\pm$ corresponding to the signs "+" and "−" in Eq. (5) as $E_\pm \equiv -k_\pm^2/2$, where $E_- > E_+$. Substituting $E_\pm = 0$ in Eq. (5), we find the critical distance R_c for which two bound states of an electron exist [32]: For $R < 1/\sqrt{\kappa_1\kappa_2}$ only one bound state is supported, while two real roots of Eq. (4) can be found for $R > 1/\sqrt{\kappa_1\kappa_2}$, and these roots approach the energies $E_j^{(0)}$ of bound s states of isolated δ centers ($k_+ \to \kappa_1$ and $k_- \to \kappa_2$) as $R \to \infty$.

For a given energy E_+ or E_-, the ratio of coefficients $c_1^{(\pm)}$ to $c_2^{(\pm)}$ can be written as

$$\frac{c_1^{(\pm)}}{c_2^{(\pm)}} = \rho_\pm \pm \sqrt{1 + \rho_\pm^2}, \quad \rho_\pm \equiv \kappa_- R\, e^{k_\pm R}. \tag{6}$$

For equivalent δ centers ($\kappa_- = 0$), the ground-state ("+") solution corresponds to the symmetric wave function $\psi_{E_+}(\mathbf{r})$ ($c_1^{(+)} = c_2^{(+)}$), while the excited-state ("−") solution determines the antisymmetric wave function $\psi_{E_-}(\mathbf{r})$ ($c_1^{(-)} = -c_2^{(-)}$) with respect to the permutation of δ centers ($\mathbf{R}_1 \leftrightarrows \mathbf{R}_2$). For nonequivalent centers ($\kappa_- \neq 0$), Eq. (6) shows that the major contribution to the wave function (1) comes from one center, while the contribution of the second one exponentially decreases with increasing R.

The absolute values of both $c_1^{(\pm)}$ and $c_2^{(\pm)}$ are fixed by the normalization condition for the wave function (1):

$$\frac{2\pi}{k_\pm}([c_1^{(\pm)}]^2 + [c_2^{(\pm)}]^2 + 2c_1^{(\pm)}c_2^{(\pm)}e^{-k_\pm R}) = 1. \tag{7}$$

The joint solution of Eqs. (6) and (7) gives

$$c_1^{(\pm)} = \sqrt{\frac{N_\pm}{4\pi}}\left[1 \pm \frac{\rho_\pm}{\sqrt{1+\rho_\pm^2}}\right]^{1/2}, \tag{8a}$$

$$c_2^{(\pm)} = \pm\sqrt{\frac{N_\pm}{4\pi}}\left[1 \mp \frac{\rho_\pm}{\sqrt{1+\rho_\pm^2}}\right]^{1/2}, \tag{8b}$$

$$N_\pm = \frac{k_\pm\sqrt{1+\rho_\pm^2}}{\sqrt{1+\rho_\pm^2} \pm e^{-k_\pm R}}. \tag{8c}$$

Note that $N_+ \to \kappa_1$, while $N_- \to \kappa_2$ for large R ($e^{-k_\pm R} \ll 1$).

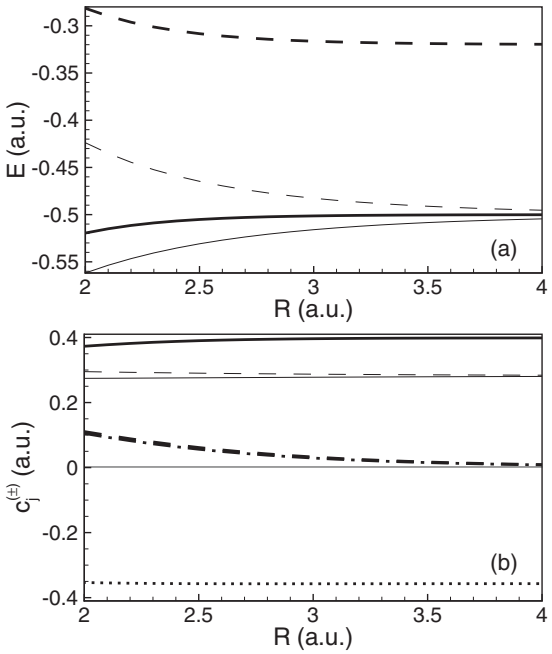

FIG. 1. Dependence of molecular model energies $E_\pm$ [cf. (5)] and wave-function coefficients $c_j^{(\pm)}$ [cf. (8)] on the distance R between two δ centers. (a) E_+ (solid lines) and E_- (dashed lines). Thin lines, equivalent centers ($\kappa_1 = \kappa_2 = 1$ a.u.); thick lines, nonequivalent centers ($\kappa_1 = 1$ a.u. and $\kappa_2 = 0.8$ a.u.). (b) Coefficients $c_j^{(\pm)}$ for the same parameters as in (a). Thin solid line, $c_1^{(+)}$ for equivalent centers ($c_2^{(+)} = c_1^{(+)}$); thin dashed line, $c_1^{(-)}$ for equivalent centers ($c_2^{(-)} = -c_1^{(-)}$); thick solid (dashed) line, $c_1^{(+)}$ ($c_2^{(+)}$) for nonequivalent centers; thick dot-dashed (dotted) line, $c_1^{(-)}$ ($c_2^{(-)}$) for nonequivalent centers. On the scale of panel (b) the dashed and dot-dashed lines are indistinguishable.

In Fig. 1(a) we present the dependence of energies $E_\pm$ on the distance between δ centers. The difference between E_+, E_- and the corresponding single-center energies $E_1^{(0)}$, $E_2^{(0)}$ is determined by the exchange interaction, i.e., by the overlap of the single-center wave functions described by the nondiagonal matrix elements in Eq. (3). Since this overlap exponentially decreases with increasing R, the energy E_+ (E_-) rapidly approaches the single-center energy $-\kappa_1^2/2$ ($-\kappa_2^2/2$). In Fig. 1(b) we show the typical dependence of the coefficients $c_j^{(\pm)}$ on R. For equivalent centers [cf. Eq. (8) for $\rho_\pm = 0$], the dependence of $c_j^{(\pm)}$ on R is weak and can be approximated as $|c_j^{(\pm)}| \approx \sqrt{\kappa_1/(4\pi)}$. For nonequivalent centers, the molecular electron in the ground state is mostly localized near the center that supports a bound state with larger binding energy $|E_j^{(0)}|$ [for $\rho_\pm \gg 1$, $c_1^{(+)} \to \sqrt{\kappa_1/(2\pi)}$, $c_2^{(+)} \to \sqrt{\kappa_1/(8\pi)}e^{-k_+R}/(\kappa_- R)$; $c_1^{(-)} \to \sqrt{\kappa_1/(8\pi)}e^{-k_-R}/(\kappa_- R)$, and $c_2^{(-)} \to -\sqrt{\kappa_1/(2\pi)}$; cf. Eq. (8)], while an electron in the excited state is mostly localized near the center with smaller $|E_j^{(0)}|$.

The continuum (scattering) states of an electron with momentum $\mathbf{p}$ and energy $E = p^2/2$ in the field of two δ potentials can be presented as a linear combination of a plane wave with momentum $\mathbf{p}$ and two spherical waves centered at

$\mathbf{R}_1$ and $\mathbf{R}_2$. Requiring this superposition to satisfy the boundary condition (2), we obtain the scattering state in the form [32]

$$(2\pi)^{3/2}\psi_{\mathbf{p}}^{(+)}(\mathbf{r}) = e^{i\mathbf{p}\cdot\mathbf{r}} - \frac{1}{\Delta(p)}\left[\left((\kappa_2+ip)e^{i\mathbf{p}\cdot\mathbf{R}_1} - \frac{e^{i\mathbf{p}\cdot\mathbf{R}_2+ipR}}{R}\right)\frac{e^{ip|\mathbf{r}-\mathbf{R}_1|}}{|\mathbf{r}-\mathbf{R}_1|} + \left((\kappa_1+ip)e^{i\mathbf{p}\cdot\mathbf{R}_2} - \frac{e^{i\mathbf{p}\cdot\mathbf{R}_1+ipR}}{R}\right)\frac{e^{ip|\mathbf{r}-\mathbf{R}_2|}}{|\mathbf{r}-\mathbf{R}_2|}\right], \quad (9)$$

where

$$\Delta(p) = (\kappa_1+ip)(\kappa_2+ip) - e^{2ipR}/R^2. \quad (10)$$

From the asymptotic form of the scattering state (9) at large distances r, we obtain the amplitude, $\mathcal{A}(\mathbf{p},\mathbf{p}')$, for elastic electron scattering by the molecular system

$$\mathcal{A}(\mathbf{p},\mathbf{p}') = \mathcal{A}_1(\mathbf{p},\mathbf{p}') + \mathcal{A}_2(\mathbf{p},\mathbf{p}'), \quad (11a)$$

$$\mathcal{A}_1(\mathbf{p},\mathbf{p}') = -\Delta(p)^{-1}e^{-i\mathbf{p}'\cdot\mathbf{R}/2}[(\kappa_2+ip)e^{i\mathbf{p}\cdot\mathbf{R}/2} - e^{-i\mathbf{p}\cdot\mathbf{R}/2}e^{ipR}/R], \quad (11b)$$

$$\mathcal{A}_2(\mathbf{p},\mathbf{p}') = -\Delta(p)^{-1}e^{i\mathbf{p}'\cdot\mathbf{R}/2}[(\kappa_1+ip)e^{-i\mathbf{p}\cdot\mathbf{R}/2} - e^{i\mathbf{p}\cdot\mathbf{R}/2}e^{ipR}/R], \quad (11c)$$

where $\mathbf{p}$ and $\mathbf{p}'$ ($=p\mathbf{r}/r$) are the initial and final asymptotic momenta, while $\mathcal{A}_1$ and $\mathcal{A}_2$ are the constituents of the electron scattering amplitude $\mathcal{A}$ originating from the two centers located at $\mathbf{R}_1 = \mathbf{R}/2$ and $\mathbf{R}_2 = -\mathbf{R}/2$. (It is easy to show that $\mathcal{A}_1$ and $\mathcal{A}_2$ reduce at large R to the scattering amplitudes for two individual δ centers.)

The shortcoming of the δ-potential model for a molecular system is that this model does not approach the limit of two "merged" δ potentials as $R \to 0$. The binding energy of the ground state tends to infinity instead of approaching a finite value. One way to overcome this shortcoming, suggested in Ref. [44], is to consider κ_1 and κ_2 as functions of R, whose two-term expansions for small R have the form $\kappa_j(R) = -\eta_j/R + \alpha_j(R)$, where $\eta_1, \eta_2 > 0$, $\eta_1\eta_2 = 1$, and $\alpha_j(R)$ are regular functions of R. For appropriately chosen η_1 and η_2, this modified δ-potential model can be extended to neutral molecules (cf. the pedagogical example for H_2 in Ref. [44]).

III. MOLECULAR MODEL IN A LASER FIELD: COMPLEX QUASIENERGIES AND QQES WAVE FUNCTIONS

In the electric-dipole approximation (length gauge) the interaction of the molecular model electron with an elliptically polarized, monochromatic laser field is

$$V(\mathbf{r},t) = \mathbf{r}\cdot\mathbf{F}(t), \quad (12)$$

where $\mathbf{F}(t)$ is the electric vector of the field with amplitude F and frequency ω,

$$\mathbf{F}(t) = F\mathrm{Re}\,(\mathbf{e}\,e^{-i\omega t}), \quad \mathbf{e}\cdot\mathbf{e}^* = 1. \quad (13)$$

The complex polarization unit vector $\mathbf{e}$ in Eq. (13) is parameterized as

$$\mathbf{e} = \frac{\hat{\boldsymbol{\epsilon}} + i\eta[\hat{\boldsymbol{\kappa}}\times\hat{\boldsymbol{\epsilon}}]}{\sqrt{1+\eta^2}}, \quad -1 \leqslant \eta \leqslant 1, \quad (14)$$

where $\hat{\boldsymbol{\epsilon}}$ is a unit vector along the major axis of the polarization ellipse, the unit vector $\hat{\boldsymbol{\kappa}}$ defines the direction of laser propagation, and η is the ellipticity. With the definition (14), the laser intensity I does not depend on η: $I = cF^2/(8\pi)$.

For a nonperturbative account of the electron's interactions with both the laser field and the two δ centers, we use the QQES (or complex quasienergy) approach [45]. In brief, instead of solving the TDSE as an initial value (Cauchy) problem, $\psi(\mathbf{r},t)|_{t=t_0} = \psi_{E_0}(\mathbf{r})\exp(-iE_0t_0)$, to determine $\psi(\mathbf{r},t)$, within the QQES approach one solves an eigenvalue problem for the complex quasienergy, $\epsilon = \mathrm{Re}\,\epsilon - i\Gamma/2$, and the periodic (in time) QQES wave function, $\Phi_\epsilon(\mathbf{r},t)$, to which E_0 and $\psi_{E_0}(\mathbf{r})$ evolve after an adiabatic turn on of the periodic strong-field interaction $V(\mathbf{r},t)$. The real and imaginary parts of the quasienergy determine the Stark-shifted energy ($\mathrm{Re}\,\epsilon = E_0 + \Delta$) and the total rate ($\Gamma$) for exponential (in time) decay of the initial bound state $\psi_{E_0}(\mathbf{r})$ in a laser field. The QQES wave function satisfies the complex, outgoing-wave boundary condition at large distances [45],

$$\Phi_\epsilon(\mathbf{r},t) \sim \sum_n A_n\frac{e^{ip_n\tilde{R}}}{\tilde{R}}, \quad \tilde{\mathbf{R}} = \mathbf{r} - \frac{\mathbf{F}(t)}{\omega^2}, \quad (15)$$

where $p_n = \sqrt{2(n\hbar\omega + \epsilon - u_p)}$ is the complex-valued "momentum" of the electron after absorption of n laser photons and $u_p = F^2/(4\omega^2)$ is the quiver energy of the electron in the monochromatic field $\mathbf{F}(t)$. In open n-photon detachment or ionization channels [$\mathrm{Re}\,(n\hbar\omega + \epsilon - u_p) > 0$], the branch of the square root for p_n is taken in the fourth quarter of the complex plane p_n ($\mathrm{Re}\,p_n > 0$, $\mathrm{Im}\,p_n < 0$) and the coefficients A_n in Eq. (15) determine the amplitudes for n-photon detachment or ionization. In closed channels [$\mathrm{Re}\,(n\hbar\omega + \epsilon - u_p) < 0$] the QQES wave function decreases exponentially and the branch of the square root for p_n is taken in the second quarter of the complex plane ($\mathrm{Re}\,p_n < 0$, $\mathrm{Im}\,p_n > 0$).

A. QQES equations for the ZRP molecular model

As for the field-free molecular model [cf. Eq. (1)], the field-dressed (QQES) wave function for an electron in the field of two δ potentials and a laser field $\mathbf{F}(t)$ can also be expressed as a linear combination of one-center wave functions,

$$\Phi_\epsilon(\mathbf{r},t) = \Phi_\epsilon^{(1)}(\mathbf{r},t) + \Phi_\epsilon^{(2)}(\mathbf{r},t). \quad (16)$$

However, as for the case of a single ZRP model in a monochromatic field [46,47], the boundary conditions for $\Phi_\epsilon(\mathbf{r},t)$ at $\mathbf{r} \to \mathbf{R}_j$ involve periodic (in time) functions $f_j(t)$ [instead of the constant coefficients c_j in Eq. (2)]:

$$\Phi_\epsilon(\mathbf{r},t)|_{\mathbf{r}\to\mathbf{R}_j} \approx \left(\frac{1}{|\mathbf{r}-\mathbf{R}_j|} - \kappa_j\right)f_j(t), \quad j = 1,2. \quad (17)$$

Each of the one-center functions $\Phi_\epsilon^{(j)}(\mathbf{r},t)$ can be expressed in terms of the function $f_j(t)$ and the retarded Green's function, $G(\mathbf{r},t;\mathbf{r}',t')$, of an electron in a laser field (cf. Refs. [19,46,47]):

$$\Phi_\epsilon^{(j)}(\mathbf{r},t) = -2\pi\int G(\mathbf{r},t;\mathbf{R}_j,t')f_j(t')e^{i\epsilon(t-t')}dt'. \quad (18)$$

The expansion of $\Phi_\epsilon^{(j)}(\mathbf{r},t)$ at $\mathbf{r}\to\mathbf{R}_j$ can be obtained in a way similar to that used for the TDER wave function in Ref. [19],

$$\Phi_\epsilon^{(j)}(\mathbf{r},t)\simeq\frac{f_j(t)}{|\mathbf{r}-\mathbf{R}_j|}+\frac{1}{\sqrt{2\pi i}}\int_0^\infty\frac{e^{iS_j(t,t-\tau)+i\epsilon\tau}f_j(t-\tau)-f_j(t)}{\tau^{3/2}}d\tau, \tag{19}$$

where $S_j(t,t')\equiv S(\mathbf{R}_j,t;\mathbf{R}_j,t')$, and the classical action for the electron in a laser field, $S(\mathbf{r},t;\mathbf{r}',t')$, has the form

$$S(\mathbf{r},t;\mathbf{r}',t')=\frac{(\mathbf{r}-\mathbf{r}')^2}{2(t-t')}+\frac{1}{c}\left[\mathbf{r}\cdot\mathbf{A}(t)-\mathbf{r}'\cdot\mathbf{A}(t')-\frac{\mathbf{r}-\mathbf{r}'}{t-t'}\int_{t'}^t\mathbf{A}(\tau)d\tau\right]-\frac{1}{2c^2}\int_{t'}^t\left[\mathbf{A}(\xi)-\frac{1}{t-t'}\int_{t'}^t\mathbf{A}(\tau)d\tau\right]^2d\xi, \tag{20}$$

where

$$\mathbf{A}(t)=\frac{cF}{\omega}\mathrm{Im}\,(\mathbf{e}\,e^{-i\omega t}) \tag{21}$$

is the vector potential of the field $\mathbf{F}(t)$. Using expansion (19) when applying the boundary condition (17) (for $j=1,2$) to the QQES wave function (16), we obtain a homogeneous system of two coupled integral equations for $f_1(t)$, $f_2(t)$ and the eigenvalue ϵ (cf. Ref. [48]):

$$-\kappa_j f_j(t)=\frac{1}{\sqrt{2\pi i}}\int_0^\infty\frac{d\tau}{\tau^{3/2}}[e^{iS(\mathbf{R}_j,t;\mathbf{R}_j,t-\tau)+i\epsilon\tau}f_j(t-\tau)-f_j(t)]+\frac{1}{\sqrt{2\pi i}}\int_0^\infty\frac{d\tau}{\tau^{3/2}}e^{iS(\mathbf{R}_j,t;\mathbf{R}_{j'},t-\tau)+i\epsilon\tau}f_{j'}(t-\tau), \tag{22}$$

where $(j,j')=(1,2)$ or $(2,1)$. Thus, for the ZRP molecular model, the eigenvalue problem for ϵ and the four-dimensional (in $\mathbf{r}$ and t) QQES wave function $\Phi_\epsilon(\mathbf{r},t)$ reduces to the system (22), since with known ϵ and $f_j(t)$ $\Phi_\epsilon(\mathbf{r},t)$ is completely determined by Eqs. (16) and (18). The functions $f_j(t)$ are the key objects of our theory since they describe the behavior of the QQES wave function $\Phi_\epsilon(\mathbf{r},t)$ near the atomic centers [cf. Eq. (17)] and the modification of molecular dynamics (including the exchange interaction) by a laser field.

An alternative form of the basic QQES equations (22) for the ZRP molecular model can be obtained by using the velocity gauge for the electron-laser interaction. It can be shown that this formulation is equivalent to representing the functions $f_j(t)$ in terms of new functions, $\hat f_j(t)$, connected to $f_j(t)$ by a unitary transformation:

$$f_j(t)=e^{i/c\{\mathbf{R}_j\cdot\mathbf{A}(t)+[1/(2c)]\int^t[\mathbf{A}^2(\xi)-\overline{\mathbf{A}^2}]d\xi\}}\hat f_j(t),\qquad\frac{\overline{\mathbf{A}^2}}{2c^2}=\frac{1}{2Tc^2}\int_0^T\mathbf{A}^2(\xi)d\xi=\frac{F^2}{4\omega^2}=u_p,\quad T=\frac{2\pi}{\omega}. \tag{23}$$

Substituting Eq. (23) into Eq. (22), we obtain homogeneous integral equations for $\hat f_j(t)$ and $\hat\epsilon=\epsilon-u_p$:

$$-\kappa_j\hat f_j(t)=\frac{1}{\sqrt{2\pi i}}\int_0^\infty\frac{d\tau}{\tau^{3/2}}[e^{i\hat S(\mathbf{R}_j,t;\mathbf{R}_j,t-\tau)+i\hat\epsilon\tau}\hat f_j(t-\tau)-\hat f_j(t)]+\frac{1}{\sqrt{2\pi i}}\int_0^\infty\frac{d\tau}{\tau^{3/2}}e^{i\hat S(\mathbf{R}_j,t;\mathbf{R}_{j'},t-\tau)+i\hat\epsilon\tau}\hat f_{j'}(t-\tau), \tag{24}$$

where

$$\hat S(\mathbf{r},t;\mathbf{r}',t')=\frac{(\mathbf{r}-\mathbf{r}')^2}{2(t-t')}-\frac{\mathbf{r}-\mathbf{r}'}{c(t-t')}\int_{t'}^t\mathbf{A}(\xi)d\xi+\frac{1}{2c^2(t-t')}\left[\int_{t'}^t\mathbf{A}(\xi)d\xi\right]^2. \tag{25}$$

Although both systems (22) and (24) are equally valid for general analyses, for numerical calculations and perturbative (in the laser intensity) analytical analyses, the system (24) is preferable, while for nonperturbative, low-frequency ($\omega\ll|E_\pm|$) analyses using the quasiclassical approximation, the system (22) is most appropriate. Indeed, analysis shows that the functions $f_j(t)$ are nearly constant in the low-frequency limit, while the functions $\hat f_j(t)$ oscillate rapidly, requiring that many Fourier coefficients of $\hat f_j(t)$ must be taken into account. For $\mathbf{F}(t)=0$, the systems (22) and (24) reduce to an infinite set of equivalent independent subsystems involving only two linear equations similar to the system (3). Thus, in the absence of a laser field, both functions $f_j(t)$ and $\hat f_j(t)$ reduce to the same constant coefficients $c_j^{(\pm)}$.

The systems of integral equations (22) and (24) can be converted to infinite systems of linear equations for the Fourier coefficients $f_k^{(j)}$ or $\hat f_k^{(j)}$ of $f_j(t)$ or $\hat f_j(t)$. For linear and circular polarizations of the field $\mathbf{F}(t)$, in Appendix A we give the matrix equations for $\hat f_k^{(j)}$, which are equivalent to the system (24) and which are useful for the perturbative (in F) analysis of the complex quasienergies and QQES wave functions.

B. Amplitude and differential rate for *n*-photon detachment

According to Eq. (15), the exact amplitude for n-photon detachment within the QQES approach can be found from the asymptotic form of the QQES wave function (16). Using the large-r asymptotic expansion of the one-center functions $\Phi_\epsilon^{(j)}(\mathbf{r},t)$ in Eq. (18) (cf. Ref. [23] for details), the amplitude A_n for the two-center molecular model has the form

$$A_n=A_n^{(1)}+A_n^{(2)}, \tag{26}$$

where $A_n^{(j)}$ is a "one-center" detachment amplitude, whose explicit forms in terms of either of the functions $f_j(t)$ or $\hat f_j(t)$ are given by

$$A_n^{(j)}=\frac{1}{T}\int_0^T e^{[iS(\mathbf{p}_n,t)-i\mathbf{P}_n(t)\cdot\mathbf{R}_j]}f_j(t)\,dt \tag{27a}$$

$$=\frac{e^{-i\mathbf{p}_n\cdot\mathbf{R}_j}}{T}\int_0^T e^{in\omega t+i\mathbf{p}_n\cdot\int^t\mathbf{A}(\tau)d\tau/c}\hat f_j(t)\,dt, \tag{27b}$$

where $\mathbf{p}_n \equiv p_n\hat{\mathbf{n}}$, where p_n is the complex canonical "momentum" [cf. Eq. (15)], $\hat{\mathbf{n}}$ is the unit vector that defines the momentum direction of the detached electron, and

$$\mathbf{P}_n(t) = \mathbf{p}_n + \frac{1}{c}\mathbf{A}(t), \tag{28}$$

$$S(\mathbf{p}_n,t) = \int^t \left[\frac{\mathbf{P}_n^2(\tau)}{2} - \epsilon\right] d\tau. \tag{29}$$

The differential rate for n-photon detachment is given by (cf. Ref. [47] for the case of a ZRP model)

$$\frac{d\Gamma_n}{d\Omega_{\hat{\mathbf{n}}}} = |\sqrt{p_n}A_n|^2. \tag{30}$$

Note that the complexity of the quasienergy ϵ is essential for obtaining the functions $f_j(t)$ or $\hat{f}_j(t)$ according to Eq. (22) or (24). However, in physical applications $|\mathrm{Im}\,\epsilon| \ll |\mathrm{Re}\,\epsilon|$. Thus, with good accuracy, in Eqs. (27a)–(30) we can replace ϵ with $\mathrm{Re}\,\epsilon$, so that the vector $\mathbf{p}_n$ then represents the physical momentum of the detached electron with $p_n = \sqrt{2(n\hbar\omega + \mathrm{Re}\,\epsilon - u_p)}$.

IV. THE WEAK-FIELD LIMIT: DYNAMIC POLARIZABILITIES FOR ψ_{E_+} AND ψ_{E_-} STATES

In this section, we analyze the weak-field limit of the general results of Sec. III. Specifically, we use PT in the amplitude F of a linearly polarized field $\mathbf{F}(t) = \mathbf{F}\cos\omega t (\mathbf{F} = \mathbf{e}F)$ to obtain the linear in the laser-intensity limit for the complex quasienergy. In this limit we obtain analytic expressions for the dynamic polarizability of the unperturbed ground $[\psi_{E_+}(\mathbf{r})]$ and excited $[\psi_{E_-}(\mathbf{r})]$ states of the two-center molecular model.

The dynamic polarizabilities $\alpha_\pm$ of the states $\psi_{E_\pm}(\mathbf{r})$ determine the leading (quadratic in F) terms in the expansion of the complex quasienergies $\epsilon_\pm$, corresponding to the unperturbed energies $E_\pm = -k_\pm^2/2$, in a PT series in F. Specifically, the complex quasienergy up to second order in F, $\epsilon_\pm^{(2)}$, is

$$\epsilon_\pm^{(2)} = -\tfrac{1}{2}k_\pm^2 - \tfrac{1}{4}\alpha_\pm F^2, \tag{31}$$

where $\alpha_\pm \equiv \alpha_\pm(\omega,R,\theta)$ and θ is the angle between $\mathbf{R}$ and $\mathbf{F}$. In Appendix B we derive the expressions for $\epsilon_\pm^{(2)}$ as approximate eigenvalues of the exact integral equation (24) presented in matrix form in Eq. (A1).

These derivations show that for an arbitrary geometry (i.e., an arbitrary angle θ) the polarizability $\alpha_\pm$ has the following parametrization:

$$\alpha_\pm = \alpha_\perp^{(\pm)}\sin^2\theta + \alpha_{||}^{(\pm)}\cos^2\theta. \tag{32}$$

Since the two-center molecular model has axial symmetry, its polarizability is a second-rank tensor. Thus, $\alpha_\perp^{(\pm)}$ and $\alpha_{||}^{(\pm)}$ are diagonal elements of this tensor and define the linear in laser-intensity corrections to the unperturbed energies $E_\pm$ for perpendicular ($\theta = 90^\circ$) and parallel ($\theta = 0^\circ$) geometries.

The explicit forms of $\alpha_\perp^{(\pm)}(\omega,R)$ and $\alpha_{||}^{(\pm)}(\omega,R)$ are (cf. Appendix B)

$$\alpha_\perp^{(\pm)}(\omega,R) = -\frac{1}{\omega^2} + \frac{N_\pm}{3\omega^4}[(2\omega + k_\pm^2)^{3/2} - 2k_\pm^3 + i(2\omega - k_\pm^2)^{3/2}] \mp \frac{N_\pm}{\omega^4}\frac{(\tilde{g}_1 + \tilde{g}_{-1})}{\sqrt{1+\rho_\pm^2}}, \tag{33a}$$

$$\alpha_{||}^{(\pm)}(\omega,R) = \alpha_\perp^{(\pm)} \mp \frac{N_\pm R}{\omega^4\sqrt{1+\rho_\pm^2}}\frac{\partial}{\partial R}(\tilde{g}_1 + \tilde{g}_{-1}) - \frac{N_\pm R}{\omega^4}\sum_{k'=\pm1}\left\{\frac{\tilde{g}_{k'}^2}{\Delta(p_{k'})}\left[R(\kappa_+ + ip_{k'}) \pm \frac{e^{ip_{k'}R} + \kappa_-^2R^2e^{k_\pm R}}{\sqrt{1+\rho_\pm^2}}\right]\right\}, \tag{33b}$$

where $\kappa_\pm = (\kappa_1 \pm \kappa_2)/2$, the R-dependent factors $\rho_\pm$ ($\rho_\pm = 0$ for $\kappa_1 = \kappa_2$), and $N_\pm$ were introduced in Eqs. (6) and (8c) for the field-free molecular model, $p_k \equiv \sqrt{2k\omega - k_\pm^2} = \sqrt{2(E_\pm + k\omega)}$ [cf. Eq. (B1)], and the factors $\tilde{g}_{k=\pm1}$ are given by [cf. Eq. (B3)]

$$\tilde{g}_k \equiv \tilde{g}_k(R,E_\pm,\omega) = \frac{1}{R}\frac{\partial}{\partial R}\frac{e^{ip_kR} - e^{-k_\pm R}}{R}. \tag{34}$$

For equivalent centers, our results [Eqs. (33a) and (33b)] after some transformations coincide with those obtained in Ref. [49] by direct calculations of second-order PT matrix elements for the polarizabilities using wave functions of the field-free molecular model described in Sec. II.

One sees that the cumbersome structures of the expressions (33a) and (33b) for $\alpha_{\perp,||}^{(\pm)}$ originate from the R-dependent terms involving the functions $\tilde{g}_{\pm1}$. With increasing R, these terms decrease as R^{-2} (for $2\omega > k_\pm^2$) or faster, so that in the limit $R \to \infty$ (in which case $N_+ = \kappa_1$, $N_- = \kappa_2$) the polarizabilities $\alpha_\perp^{(\pm)}$ and $\alpha_{||}^{(\pm)}$ become equal and tend toward the dynamic polarizabilities $\alpha_{\kappa_j}^{\mathrm{ZRP}}$ of individual δ centers characterized by the parameters κ_j ($\kappa_1 \geqslant \kappa_2$) [36,50]:

$$\alpha_{\kappa_j}^{\mathrm{ZRP}}(\omega) = \lim_{R\to\infty}\alpha_\perp^{(\pm)} = \lim_{R\to\infty}\alpha_{||}^{(\pm)} = -\frac{1}{\omega^2} + \frac{\kappa_j}{3\omega^4}\left[\left(2\omega + \kappa_j^2\right)^{3/2} - 2\kappa_j^3 + i\left(2\omega - \kappa_j^2\right)^{3/2}\right]. \tag{35}$$

A. The plane-wave approximation for $\alpha_\pm(\omega,R)$

To clarify the origin of the different terms in the expressions (33a) and (33b), which provide the laser-field-dependent contributions to the complex quasienergies $\epsilon_\pm^{(2)}$ in Eq. (31) (including an exact account of both the potentials of the individual short-range centers and the exchange interaction effects), it is useful to compare Eqs. (33a) and (33b) with a less exact result. For the latter, consider the polarizabilities $\alpha_\pm^{(\mathrm{pw})}$ of the states $\psi_{E_\pm}(\mathbf{r})$ in Eq. (1) in the plane-wave approximation (PWA), using the velocity gauge for the operator $V(\mathbf{r},t)$,

$$\alpha_\pm^{(\mathrm{pw})} = -\omega^{-2}\left[1 - \langle\psi_{E_\pm}|VG_{E_\pm+\omega}^{(0)}V|\psi_{E_\pm}\rangle - \langle\psi_{E_\pm}|VG_{E_\pm-\omega}^{(0)}V|\psi_{E_\pm}\rangle\right], \tag{36}$$

where $V = (\mathbf{e}\cdot\hat{\mathbf{p}})$, $\mathbf{e} = \mathbf{F}/F$, $\hat{\mathbf{p}} = -i\boldsymbol{\nabla}$, and $G_{\mathcal{E}}^{(0)} = e^{i\sqrt{2\mathcal{E}}|\mathbf{r}-\mathbf{r}'|}/(2\pi|\mathbf{r}-\mathbf{r}'|)$ is the outgoing-wave Green's function of a free electron. Thus, in the PWA we neglect spherical waves in the scattering state (9), as well as the contribution of the bound state $\psi_{E_-}(\mathbf{r})$ [or $\psi_{E_+}(\mathbf{r})$] when calculating $\alpha_+^{(\mathrm{pw})}$ (or $\alpha_-^{(\mathrm{pw})}$). After calculating the integrals in Eq. (36) (which is simplest in the momentum representation), the

result for $\alpha_{\pm}^{(\mathrm{pw})}$ acquires the form (32), where $\alpha_{\perp}^{(\pm)}$ and $\alpha_{||}^{(\pm)}$ are replaced with their PWA counterparts, $\alpha_{\perp}^{(\pm,\mathrm{pw})}$ and $\alpha_{||}^{(\pm,\mathrm{pw})}$. Moreover, $\alpha_{\perp}^{(\pm,\mathrm{pw})}$ coincides with the exact result in Eq. (33a), i.e., $\alpha_{\perp}^{(\pm,\mathrm{pw})} = \alpha_{\perp}^{(\pm)}$, while $\alpha_{||}^{(\pm,\mathrm{pw})}$ is given by Eq. (33b) with omission of the terms $\propto g_k^2$. These latter beyond-PWA terms in Eq. (33b) describe the much more complicated frequency and R dependencies of the polarizabilities $\alpha_{||}^{(\pm)}$ as compared to $\alpha_{||}^{(\pm,\mathrm{pw})}$, as well as the resonant behavior of $\alpha_{||}^{(\pm)}$ for frequencies $\omega \approx (E_- - E_+)$ (cf. Sec. VI).

The PWA analysis provides clear interpretations of the individual terms in Eq. (33a) for $\alpha_{\perp}^{(\pm)}(\omega, R)$. The terms in brackets originate from "diagonal" matrix elements in Eq. (36) with functions $\psi_{E_\pm}^{(1)}$ or $\psi_{E_\pm}^{(2)}$ instead of $\psi_{E_\pm}$ [cf. Eq. (1)] and take into account exchange interaction effects only on the minimal, zero-field level (by means of $N_\pm$). For large R, these terms in Eqs. (33a) and (33b) become the polarizabilities (35) of individual δ centers. The last term in Eq. (33a), involving $\tilde{g}_1 + \tilde{g}_{-1}$, corresponds to "nondiagonal" matrix elements in Eq. (36) with functions $\psi_{E_\pm}^{(1)}$ and $\psi_{E_\pm}^{(2)}$. For $\alpha_{||}^{(\pm)}$, this term in Eq. (33a) for $\alpha_{\perp}^{(\pm)}$ joins with the last term in the first line of Eq. (33b) to form the combination $\partial[R(\tilde{g}_1 + \tilde{g}_{-1})]/\partial R$. These "interference" terms originate solely from the exchange interaction and exhibit exponential and (for $2\omega > k_\pm^2$) oscillatory dependence on the laser frequency [cf. Eq. (34)]. The coincidence of exact and PWA results for $\alpha_{\perp}^{(\pm)}$ is not surprising in view of the selection rules for dipole transitions in our two-center system: While the angular momentum is not conserved in this case, its projection m on the quantization axis z directed along the vector $\mathbf{R}$ is a good quantum number. Thus, for dipole transitions in a linearly polarized field, the selection rule for orthogonal geometry ($\mathbf{e} \cdot \mathbf{R} = 0$) is $|\Delta m| = 1$. For this reason, a one-photon transition from the unperturbed states $\psi_{E_\pm}$ is possible only to the p-wave channel of the plane wave $\exp(i\mathbf{p} \cdot \mathbf{r})$ in the scattering state (9). For similar reasons, a dipole transition between the states ψ_{E_+} and ψ_{E_-} is forbidden for the case of orthogonal geometry.

B. The static-field limit for $\alpha_{\pm}(\omega, R, \theta)$

Expanding the expressions (33a) and (33b) (including $\tilde{g}_k$) in series in ω for small ω up to terms $\sim\omega^4$, one obtains (after lengthy but straightforward algebra) static-field results for $\alpha_{\perp,\parallel}^{(\pm)}(\omega, R)$, which we present separately for nonequivalent ($\kappa_1 > \kappa_2$) and equivalent ($\kappa_1 = \kappa_2$) δ centers. For the former, the results for $\alpha_{\perp,\parallel}^{(\pm)}(0, R)$ are

$$\alpha_{\perp}^{(\pm)}(0,R) = \frac{N_\pm}{4k_\pm^5}\left[1 \pm \frac{e^{-k_\pm R}}{\sqrt{1+\rho_\pm^2}}\left(1 + k_\pm R + \frac{k_\pm^2 R^2}{3}\right)\right], \tag{37a}$$

$$\alpha_{\parallel}^{(\pm)}(0,R) = \alpha_{\perp}^{(\pm)}(0,R) + \frac{N_\pm R^2}{4k_\pm^3}\left\{1 \pm \frac{k_\pm R e^{k_\pm R}}{\sqrt{1+\rho_\pm^2}} - 4d_0^2\left[1 \pm \frac{k_\pm R e^{k_\pm R} + (1 - 2k_\pm R)\, e^{-k_\pm R}}{\sqrt{1+\rho_\pm^2}}\right]\right\}, \tag{37b}$$

where

$$d_0 = \pm\frac{\rho_\pm N_\pm}{2k_\pm\sqrt{1+\rho_\pm^2}} = \frac{\kappa_- R}{2(e^{-2k_\pm R} \pm \sqrt{e^{-2k_\pm R} + \kappa_-^2 R^2})}. \tag{38}$$

Note that the results in Eqs. (37a) and (37b) coincide with the TDER results of Ref. [34] for a two-center system in a static electric field $\mathbf{F}$ (neglecting there the effective ranges $r_0^{(1)}$ and $r_0^{(2)}$ of the two atomic centers [51]).

For identical centers ($\rho_\pm = 0$, $d_0 = 0$), the results for $\alpha_{\perp,\parallel}^{(\pm)}(0, R)$ reduce to those obtained in Ref. [33]:

$$\alpha_{\perp}^{(\pm)}(0,R)|_{\kappa_1=\kappa_2} = \frac{N_\pm}{4k_\pm^5}\left(1 \pm e^{-k_\pm R}\left[1 + k_\pm R + \frac{k_\pm^2 R^2}{3}\right]\right), \tag{39a}$$

$$\alpha_{\parallel}^{(\pm)}(0,R)|_{\kappa_1=\kappa_2} = \alpha_{\perp}^{(\pm)}(0,R)|_{\kappa_1=\kappa_2} + \frac{N_\pm R^2}{4k_\pm^3}(1 \pm k_\pm R e^{k_\pm R}). \tag{39b}$$

Comparison of the results in Eqs. (37) and (39) with those in Eqs. (33a) and (33b) is instructive in two respects. First, it shows how the exchange interaction is modified by an alternating electric field as compared to the case of a true static field $\mathbf{F}$. The factors $\tilde{g}_k$ in Eq. (34), which describe the effects of the exchange interaction, become frequency-dependent in an alternating field $\mathbf{F}(t)$. Whereas they are exponentially decreasing in R (as for the case of a static field) for $\omega < k_\pm^2/2$ (when both p_1 and p_{-1} are purely imaginary), the factor $\tilde{g}_{k=1}$ acquires an oscillating (in R) component for $\omega > k_\pm^2/2$ (when the one-photon detachment channel becomes open and p_1 gives the momentum of the detached electron). Furthermore, the decrease of this component with increasing R is much slower ($\propto R^{-2}$) than the exponential decrease of the component involving $e^{-k_\pm R}$ in Eq. (34). Second, the parallel polarizability (37b) involves the parameter $d_0 \sim \kappa_-$, which determines a permanent dipole moment, $\mathbf{d}_0 = d_0\mathbf{R}$, of a heteropolar two-center system [as can also be verified by straightforward calculation of the matrix element $\langle\psi_{E_\pm}|\mathbf{r}|\psi_{E_\pm}\rangle$ with the zero-field wave function (1)]. However, the frequency-dependent result (33b) for $\alpha_{\parallel}^{(\pm)}(\omega, R)$ does not involve any features related to the permanent dipole moment $\mathbf{d}_0$: These features appear only after expansion of the beyond-PWA (i.e., containing $\tilde{g}_{\pm1}^2$) terms in Eq. (33b) in a series in ω. Moreover, in a static electric field $\mathbf{F}$, the PT expansion of field-induced corrections to the unperturbed energies $E_\pm$ besides the quadratic Stark-shift contains also the linear Stark-shift given by the term $-(\mathbf{d}_0 \cdot \mathbf{F})$ [34], while the weak-field expansion of the quasienergy in Eq. (31) is valid for any nonzero frequency ω and remains quadratic in the field amplitude F.

For a system having a permanent dipole moment, the question of the manifestation of linear Stark effect features with decreasing frequency ω of an alternating field $\mathbf{F}(t)$ with a given amplitude F was studied long ago in Ref. [52] (for a polar molecule) and Refs. [52,53] (for the hydrogen atom in an excited state). As shown in Ref. [52], for a polar molecule in a linearly polarized, low-frequency field $\mathbf{F}(t)$ these features become pronounced in the spectrum of "quasienergy harmonics" [or Fourier coefficients $\Phi_\epsilon^{(n)}(\mathbf{r})$] of the QQES

wave function $\Phi_\epsilon(\mathbf{r},t)$ when the condition, $|\mathbf{d_0}\cdot\mathbf{F}| \gtrsim \omega$, is fulfilled, i.e., when the photon energy is comparable with (or smaller than) the maximum value of the dipole interaction, $-\mathbf{d_0}\cdot\mathbf{F}(t)$, of a molecule with an oscillating field $\mathbf{F}(t)$. The ordinary PT approach used in this section for analysis of the complex quasienergy ϵ based on the integral equations (24) is not appropriate for a proper analysis of effects caused by a permanent dipole moment. The most appropriate approach for this purpose is an analysis of the integral equations (22) in the low-frequency (quasiclassical) limit. However, this latter analysis is beyond the scope of this paper and will be published elsewhere.

V. THE WEAK-FIELD LIMIT: PHOTODETACHMENT CROSS SECTIONS FOR THE ψ_{E_+} AND ψ_{E_-} STATES

Besides the quadratic Stark shift of the energy of a bound state in a monochromatic light field, the dynamic polarizability tensor also determines the amplitude for elastic photon scattering by a bound system [54]. For $\omega > k_\pm^2/2$, the one-photon detachment channel becomes open and the polarizability $\alpha_\pm(\omega)$ acquires an imaginary part that determines the total (i.e., integrated over the angular distribution of the detached electron) photodetachment cross section, $\sigma_\pm$, according to the optical theorem for the elastic photon scattering amplitude [54]:

$$\sigma_\pm = \frac{4\pi\omega}{c}\mathrm{Im}\alpha_\pm. \tag{40}$$

It follows from the parametrization (32) for $\alpha_\pm$ that the total detachment cross section has a similar parametrization (cf. Ref. [55]):

$$\sigma_\pm = \sigma_{||}^{(\pm)}\cos^2\theta + \sigma_\perp^{(\pm)}\sin^2\theta, \tag{41}$$

where $\sigma_{||}^{(\pm)}$ and $\sigma_\perp^{(\pm)}$ are the detachment cross sections for parallel and perpendicular orientations of the molecular axis $\mathbf{R}$ with the direction of linear laser polarization $\mathbf{e} = \mathbf{F}/F$. The explicit forms of $\sigma_\perp^{(\pm)}$, $\sigma_{||}^{(\pm)}$ can be obtained from Eqs. (33a) and (33b) and are discussed in Sec. VI.

To obtain the angular distribution of the detached electron, we use the exact QQES amplitude (26) for n-photon detachment. Expanding the amplitudes (27b) with $j = 1$ and 2 up to terms linear in F and using the explicit form (B4) for the coefficients $\hat{f}_1^{(j)}$, we obtain the amplitude $A_1^{(\pm)}(\mathbf{p})$ for angle-resolved one-photon detachment from the states $\psi_{E_\pm}(\mathbf{r})$ as

$$A_1^{(\pm)}(\mathbf{p}) = \frac{F}{2\omega^2}\left[c_1^{(\pm)}A_1^{(1)}(\mathbf{p}) + c_2^{(\pm)}A_1^{(2)}(\mathbf{p})\right], \tag{42a}$$

$$A_1^{(1)} = [i(\mathbf{e}\cdot\mathbf{p}) - (\mathbf{e}\cdot\mathbf{R})\tilde{g}_1\mathcal{A}_2(-\mathbf{p},\mathbf{p})]\,e^{-i\mathbf{p}\cdot\mathbf{R}/2}, \tag{42b}$$

$$A_1^{(2)} = [i(\mathbf{e}\cdot\mathbf{p}) + (\mathbf{e}\cdot\mathbf{R})\tilde{g}_1\mathcal{A}_1(-\mathbf{p},\mathbf{p})]\,e^{i\mathbf{p}\cdot\mathbf{R}/2}, \tag{42c}$$

where $\mathbf{p}$ is the momentum of the detached electron, $p = \sqrt{2\omega - k_\pm^2} = \sqrt{2(E_\pm + \omega)}$, and two constituents of the electron scattering amplitude $\mathcal{A}$, $\mathcal{A}_1$ and $\mathcal{A}_2$, are given by Eqs. (11b) and (11c). From these equations follows an important symmetry relation between $\mathcal{A}_1$ and $\mathcal{A}_2$ for the case of equivalent atomic centers ($\kappa_- = 0$),

$$\mathcal{A}_1(-\mathbf{p},\mathbf{p}) = \mathcal{A}_2(\mathbf{p},-\mathbf{p}), \tag{43}$$

while the similar relation for nonequivalent centers is

$$\mathcal{A}_1(-\mathbf{p},\mathbf{p}) = \mathcal{A}_2(\mathbf{p},-\mathbf{p}) - \frac{\kappa_-}{\Delta(p)}e^{-i\mathbf{p}\cdot\mathbf{R}}. \tag{44}$$

Equation (43) leads to the symmetry relation, $A_1^{(1)}(\mathbf{p}) = -A_1^{(2)}(-\mathbf{p})$, for the partial amplitudes $A_1^{(j)}(\mathbf{p})$. As a result, it gives also the following symmetry relation for the detachment amplitude (42a) for equivalent centers ($c_1^{(\pm)} = \pm c_2^{(\pm)}$):

$$A_1^{(\pm)}(\mathbf{p}) = \mp A_1^{(\pm)}(-\mathbf{p}). \tag{45}$$

Using the amplitude (42a), the differential cross section for one-photon detachment can be obtained from the general result (30) for the differential n-photon detachment rate, $d\Gamma_n/d\Omega$:

$$\frac{d\sigma_\pm}{d\Omega} = \frac{8\pi\omega}{cF^2}\frac{d\Gamma_1}{d\Omega} = \frac{8\pi\omega p}{cF^2}|A_1^{(\pm)}(\mathbf{p})|^2 = \frac{2\pi p}{c\omega^3}\left|c_1^{(\pm)}A_1^{(1)}(\mathbf{p}) + c_2^{(\pm)}A_1^{(2)}(\mathbf{p})\right|^2. \tag{46}$$

The two terms in each of Eqs. (42b) and (42c) describe two contributions (having different physical origins) to the amplitudes $A_1^{(1)}$ and $A_1^{(2)}$. The first term (proportional to $\mathbf{e}\cdot\mathbf{p}$) in $A_1^{(1)}$ (or $A_1^{(2)}$) describes a one-photon transition from the first, $\psi_{E_\pm}^{(1)}$ (or second, $\psi_{E_\pm}^{(2)}$), constituent of the bound state (1) to the plane-wave part of the scattering state (9), while the second term (proportional to $\mathbf{e}\cdot\mathbf{R}$) describes the transition to the spherical wave of the scattering state (9) with origin at $\mathbf{R}_2$ (or $\mathbf{R}_1$). Thus, this term describes the beyond-PWA interaction of an electron detached from one center with the other center. Therefore, photodetachment of a two-center molecular system may be considered as involving two pairs of interfering pathways: two "direct" (or "PWA") paths, involving detachment from each of the two atomic centers, and two paths, each involving detachment from one center followed by interaction of the detached electron with the other center.

For equivalent centers ($\kappa_1 = \kappa_2 \equiv \kappa$), the photodetachment cross sections (46) for the ground ($c_1^{(+)} = c_2^{(+)}$) and excited ($c_1^{(-)} = -c_2^{(-)}$) states take relatively simple forms owing to the symmetry relation (43):

$$\frac{d\sigma_\pm}{d\Omega} = \frac{d\sigma_\pm^{(\mathrm{pw})}}{d\Omega} + \frac{N_\pm p}{c\omega^3}(\mathbf{e}\cdot\mathbf{R})\{2\mathrm{Re}\,\mathcal{G}_\pm(\mathbf{e}\cdot\mathbf{p})\sin(\mathbf{p}\cdot\mathbf{R}) + |\mathcal{G}_\pm|^2(\mathbf{e}\cdot\mathbf{R})[1\mp\cos(\mathbf{p}\cdot\mathbf{R})]\}, \tag{47}$$

where

$$\frac{d\sigma_\pm^{(\mathrm{pw})}}{d\Omega} = \frac{N_\pm p}{c\omega^3}(\mathbf{e}\cdot\mathbf{p})^2\left[1\pm\cos(\mathbf{p}\cdot\mathbf{R})\right], \tag{48}$$

$$\mathcal{G}_\pm = \frac{\tilde{g}_1}{\kappa + ip \mp e^{ipR}/R}. \tag{49}$$

Expression (48) is the differential cross section in the PWA (or Born approximation), i.e., neglecting spherical waves in the scattering state (9). Note that the exact cross section (47) is valid for any geometry and reduces to the PWA result only for orthogonal geometry ($\mathbf{e}\cdot\mathbf{R} = 0$).

In agreement with the symmetry relation (45), the explicit form (47) of $d\sigma_\pm/d\Omega$ shows that the detached electron angular distribution for the case of equivalent atomic centers has inversion symmetry with respect to the momentum $\mathbf{p}$. This is similar to the case of a single-center problem, such as

atomic photoionization. In general, this symmetry vanishes for the case of nonequivalent centers [cf. Eq. (44)]. However, even in this case it exists for orthogonal geometry ($\mathbf{e}\cdot\mathbf{R}=0$), for which only the plane-wave part of the scattering state (9) contributes to the amplitude $A_1^{(\pm)}(\mathbf{p})$ and the exact detachment cross section (46) coincides with that in the PWA:

$$\frac{d\sigma_\perp^{(\pm)}}{d\Omega}=\frac{N_\pm p}{c\omega^3}(\mathbf{e}\cdot\mathbf{p})^2\left[1\pm\frac{\cos(\mathbf{p}\cdot\mathbf{R})}{\sqrt{1+\rho_\pm^2}}\right]. \tag{50}$$

Thus, Eq. (50) presents the general PWA result for the detachment cross section (46) for any geometry including the result (48) as a special case for $\rho_\pm=0$ [cf. Eq. (6) for $\kappa_-=0$].

VI. NUMERICAL RESULTS AND DISCUSSION

A. Identical ZRP centers ($\kappa_1=\kappa_2\equiv\kappa$)

In Figs. 2 and 3, we present results for the frequency dependence of the polarizabilities $\alpha_{||,\perp}^{(\pm)}(\omega,R)$ for two values of R (small and large). [Instead of $\mathrm{Im}\,\alpha_{||,\perp}$, we use the total photodetachment cross section, $\sigma_{||,\perp}^{(\pm)}$, related to $\mathrm{Im}\,\alpha_{||,\perp}$ according to Eq. (40).] One sees a number of marked differences between the exact results for $\alpha_{||}^{(\pm)}$ and $\alpha_\perp^{(\pm)}$, as well as between the exact and PWA results for $\alpha_{||}^{(\pm)}$ (recall that $\alpha_\perp^{(\pm)}=\alpha_\perp^{(\pm,\mathrm{pw})}$). In what follows, we discuss these differences in turn.

1. Resonant features in the polarizabilities $\alpha_{||}^{(\pm)}(\omega,R)$

For orthogonal geometry ($\mathbf{e}\cdot\mathbf{R}=0$), the frequency dependencies of both $\mathrm{Re}\,\alpha_\perp^{(\pm)}(\omega,R)$ and $\sigma_\perp^{(\pm)}(\omega,R)$ are relatively smooth and qualitatively similar to that for a single δ center [cf. Eq. (35) with $\kappa_j=\kappa$], and this similarity becomes more distinct with increasing R [cf. Fig. 2]. However, for parallel geometry ($\mathbf{e}\,||\,\mathbf{R}$), the frequency dependence of $\alpha_{||}^{(\pm)}(\omega,R)$ differs crucially from the case $\mathbf{e}\cdot\mathbf{R}=0$ for both below-threshold ($\omega<|E_\pm|$) and above-threshold ($\omega>|E_\pm|$) frequencies (cf. Fig. 3). For moderate R (when the exchange interaction effects are significant), the behavior of $\mathrm{Re}\,\alpha_{||}^{(\pm)}(\omega,R)$ is governed predominantly by the contribution of the second bound state, ψ_{E_-} for $\alpha_{||}^{(+)}$ or ψ_{E_+} for $\alpha_{||}^{(-)}$, which are neglected in the PWA result (36). The straightforward calculation of the matrix element for a dipole transition between states ψ_{E_+} and ψ_{E_-} gives

$$\langle\psi_{E_-}|\mathbf{e}\cdot\hat{\mathbf{p}}|\psi_{E_+}\rangle=i(\mathbf{e}\cdot\mathbf{R})\frac{\sqrt{N_+N_-}}{\omega_r}g_1(R,E_+,\omega_r), \tag{51}$$

where $\omega_r=(k_+^2-k_-^2)/2=E_--E_+$. Note that only "nondiagonal" transitions [between constituents $\psi_{E_\pm}^{(1)}$ and $\psi_{E_\pm}^{(2)}$ of the wave function (1); cf. discussion below Eq. (36)] contribute to the matrix element (51). Since these transitions are exchange-interaction-induced [cf. the factor $g_1(R,E_+,\omega_r)$ in Eq. (51)], the matrix element (51) should vanish in the limit $R\to\infty$. The result (51) is valid for both equivalent and nonequivalent centers, while in the former case it allows a further simplification. For this case, expanding the factor $g_1(R,E_+,\omega_r)$ [cf. Eq. (34) with $ip_{k=+1}=-k_-$] for large R, we obtain an estimate,

$$\langle\psi_{E_-}|\mathbf{e}\cdot\hat{\mathbf{p}}|\psi_{E_+}\rangle\approx i\omega_r(\mathbf{e}\cdot\mathbf{R}), \tag{52}$$

where the frequency ω_r decreases exponentially with increasing R [cf. Eq. (5) and Fig. 1]. For near-resonant frequencies, the dominant term in the polarizability $\alpha_\pm(\omega)$ in Eq. (32) is

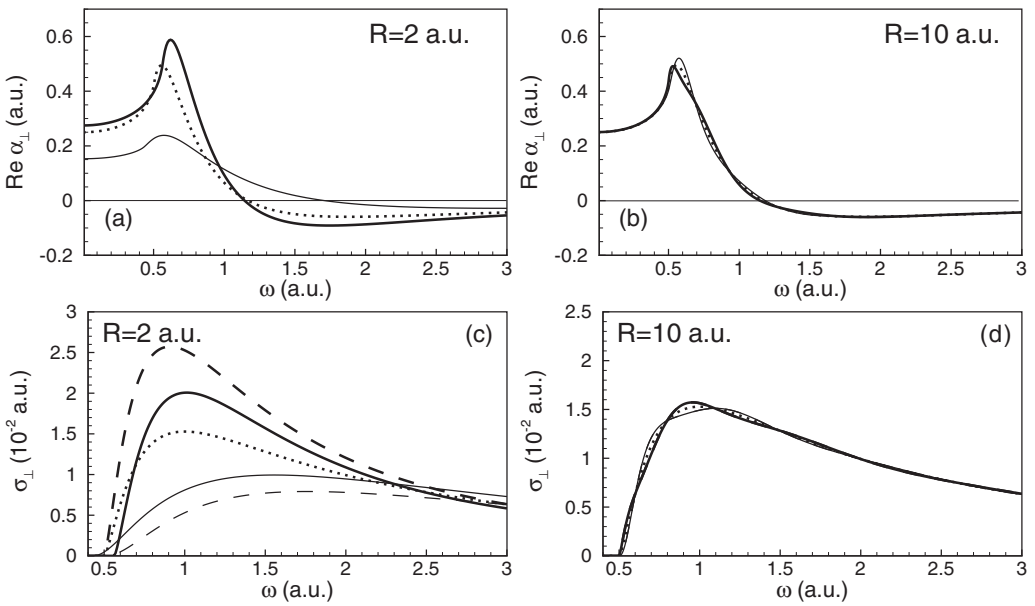

FIG. 2. Dependence of the real part of $\alpha_\perp$ (a),(b) and $\sigma_\perp$ (c),(d) on ω for $\kappa_1=\kappa_2=1$ a.u. and two values of R. Solid thick lines, results for the ground state ψ_{E_+}; solid thin lines, results for the excited state ψ_{E_-}; dotted lines, results for a single δ center. In (c),(d) the dashed thick (thin) lines are the results for $\sigma_\perp^{(\pm)}(\omega,R)$ of Refs. [39–41] [see text below Eq. (61) for discussion] for the ground (excited) state, with proper normalization of the ground (excited) state wave functions.

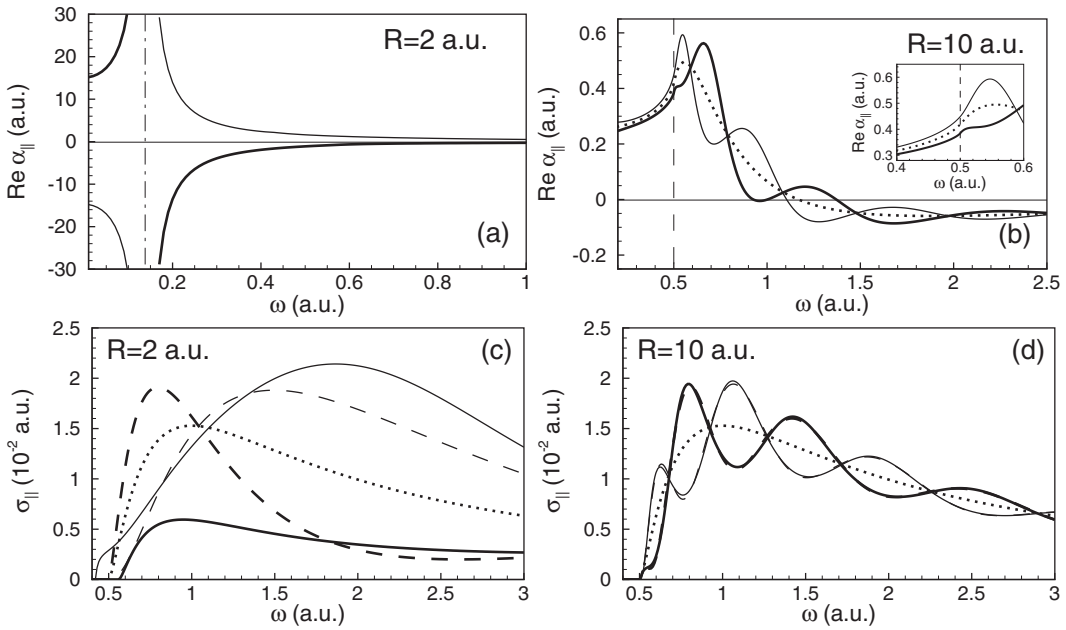

FIG. 3. The same as in Fig. 2 but for $\alpha_{||}$ and $\sigma_{||}$. The vertical dash-dotted line in (a) marks the position of the resonant frequency, $\omega_r = 0.138$ a.u. The vertical dashed line in (b) marks the position of the one-photon threshold for the ground state.

given by the expression

$$\alpha_{\pm} \propto \pm \frac{|\langle \psi_{E_-} | \mathbf{e}\cdot\hat{\mathbf{p}} | \psi_{E_+}\rangle|^2}{\omega - (E_- - E_+)} \tag{53}$$

$$= \pm(\mathbf{e}\cdot\mathbf{R})^2 \frac{N_+ N_- g_1^2(R, E_+, \omega_r)}{\omega_r^2(\omega - \omega_r)}, \tag{54}$$

which describes the resonant features in Fig. 3(a). [Note that the resonant term (54) for $\mathbf{e} \,||\, \mathbf{R}$ follows also from the exact result (33b) for $\alpha_{||}^{(\pm)}(\omega, R)$ by considering there the limit $\omega \to \omega_r$; in this case, the resonant denominator $\omega - \omega_r$ in Eq. (54) originates from expansion of the factor $\Delta(p_{+1})$ about $\omega = \omega_r$.] In agreement with the estimate (52), the resonance becomes more narrow with increasing R, its position moves to the low-frequency region, and resonant features completely disappear in the limit $R \to \infty$. We note that the ordinary PT approach, used in this paper, is not applicable for analytic analysis of resonant features in polarizabilities for close-to-resonance frequencies (including the case of an exact resonance, $\omega = \omega_r$). Such analysis requires the use of a modification of PT for treatment of almost degenerate or resonant levels within the QQES approach (cf., e.g., Refs. [50,56]). We do not pursue this question in the present paper.

2. *Oscillation patterns*

In the case of small R, the beyond-PWA effects for $\alpha_{||}^{(\pm)}$ are very significant, causing resonant features in the frequency dependence of $\mathrm{Re}\,\alpha_{||}^{(\pm)}$ and considerable differences between exact and PWA results for the photodetachment cross sections $\sigma_{||}^{\pm}$ [cf. Fig. 3(c)]. In contrast, the most prominent features for the case of large R are oscillation patterns in the frequency dependence of both $\mathrm{Re}\,\alpha_{||}^{(\pm)}$ for above-threshold frequencies ($\omega > |E_{\pm}|$) and the cross sections $\sigma_{||}^{\pm}$ [cf. Figs. 3(b) and 3(d)]. These are well described already in the PWA, at least, for far-from-threshold frequencies and/or large R.

For parallel geometry, the exact result for the cross section $\sigma_{||}^{(\pm)}$ can be presented in factorized form after integration of Eq. (47) over the momentum directions:

$$\sigma_{||}^{(\pm)} = \sigma_0^{(\pm)} f_{||}^{(\pm)}(pR), \tag{55}$$

where the first factor,

$$\sigma_0^{(\pm)} = \frac{4\pi N_{\pm}}{3c\omega^3} p^3, \quad p = \sqrt{2E} = \sqrt{2\omega - k_{\pm}^2}, \tag{56}$$

reduces to the detachment cross section $\sigma_{\kappa}^{\mathrm{ZRP}}$ for a single ZRP model [cf. Eq. (35)] for $R \to \infty$ (when both $N_{\pm}, k_{\pm} \to \kappa$), while the modulation function $f_{||}^{(\pm)}(x)$ involves the spherical Bessel functions $j_l(x)$ describing oscillation patterns:

$$f_{||}^{(\pm)}(x) = 1 \pm \frac{3}{x} j_1(x) \mp 3 j_2(x) + 6\frac{R}{p}\mathrm{Re}\,\mathcal{G}_{\pm} j_1(x) + 3\frac{R^2}{p^2}|\mathcal{G}_{\pm}|^2[1 \mp j_0(x)], \tag{57}$$

where $\mathcal{G}_{\pm}$ is given by Eq. (49).

The PWA result for $\sigma_{||}^{(\pm)}$ follows from Eq. (55) neglecting terms with $\mathcal{G}_{\pm}$ in Eq. (57):

$$\sigma_{||}^{(\pm,\mathrm{pw})} = \sigma_0^{(\pm)} f_{||}^{(\pm,\mathrm{pw})}(pR), \tag{58}$$

$$f_{||}^{(\pm,\mathrm{pw})}(x) = 1 \pm 3\left(\frac{\sin x}{x} + 2\frac{\cos x}{x^2} - 2\frac{\sin x}{x^3}\right). \tag{59}$$

Since $\sigma_{\perp}^{(\pm)} = \sigma_{\perp}^{(\pm,\mathrm{pw})}$, a factorization similar to (58) for the perpendicular geometry is exact:

$$\sigma_{\perp}^{(\pm)} = \sigma_0^{(\pm)} f_{\perp}^{(\pm)}(pR), \tag{60}$$

$$f_{\perp}^{(\pm)}(x) = 1 \pm \frac{3}{x} j_1(x) = 1 \pm \frac{3}{x^2}\left(\frac{\sin x}{x} - \cos x\right). \tag{61}$$

For the ground state ψ_{E_+}, the modulation functions $f_{||,\perp}^{(+,\mathrm{pw})}(x)$ in Eqs. (59) and (61) coincide with results obtained in Refs. [39–41] using a simplified two-center model for photodetachment of a negative molecular ion, while instead of R-dependent cross sections $\sigma_0^{(\pm)}$, the results in Refs. [39–41] contain the ZRP cross section $\sigma_\kappa^{\mathrm{ZRP}}$ with $k_\pm = \kappa$; i.e., Refs. [39–41] neglect exchange interactions in both ground and scattering states. [As is seen in Figs. 2(c) and 2(d) and Figs. 3(c) and 3(d), this difference is considerable only for small R.]

For $\omega > |E_\pm|$, an oscillatory dependence of both $\mathrm{Re}\,\alpha_{||}^{(\pm)}$ and $\mathrm{Im}\,\alpha_{||}^{(\pm)}$ on the parameter pR causes interference fringes in the frequency dependence of $\mathrm{Re}\,\alpha_{||}^{(\pm)}$ and $\sigma_{||}^{(\pm)}$, as seen in Figs. 3(b) and 3(d). Moreover, these fringes become pronounced only for those R and ω (or p), for which the de Broglie wavelength, $\lambda = 2\pi/p$, becomes of the order of (or smaller than) the interatomic distance R, thereby providing clear evidence for the double-slit origin of the oscillation patterns. The original idea to observe Young's double-slit interferences in photoionization of homonuclear diatomic molecules was proposed by Cohen and Fano [57], who obtained a remarkably simple result for the interference factor, $1 + \sin(pR)/(pR)$, in the total photoionization cross section for the case of randomly oriented molecules. [This result follows also by averaging σ_+ in Eq. (41) taking into account Eqs. (59) and (61) [39–41]. For the excited state, a similar averaging of σ_- gives the interference factor $1 - \sin(pR)/(pR)$.] Double-slit interferences in angular distributions of fast photoelectrons for a fixed-in-space molecule were predicted for the first time by Kaplan and Markin [58] within the PWA analysis for H_2 taking into account nondipole effects. Recently, the first direct experimental observation of Young's double-slit interferences in vibrationally resolved photoionization of homo- and heteronuclear diatomic molecules has been reported [59].

To estimate the positions of the maxima and minima in the R-dependence of the total cross section $\sigma_{||}$, we take into account only the first two terms in the modulation function (59) for large x. In this approximation we obtain

$$pR_{\mathrm{max\,/\,min}} = \pi(n + 1/2), \tag{62}$$

where even (odd) n correspond to the maxima of $\sigma_{||}$ for the ground (excited) state, while odd (even) n determine the minima for the ground (excited) state. In Fig. 4 we demonstrate the accuracy of the estimate (62), as well as the comparison of exact and PWA results for the R dependence of $\sigma_{||}$ for two laser frequencies. One sees that for near-threshold frequencies [cf. Fig. 4(a)] both the PWA and estimate (62) become applicable only for large R. However, for large frequencies [cf. Fig. 4(b)] the PWA and the exact results agree well even for small R, while the positions of the maxima/minima agree with Eq. (62), showing that the oscillation pattern in the R dependence of $\sigma_{||}$ originates from double-slit interference in the angular distribution of the detached electrons.

While the features of double-slit interferences are not visible in Figs. 2(c) and 2(d) for orthogonal geometry [in view of the damping factor $x^{-2} \equiv (pR)^{-2}$ in Eq. (61)], they become pronounced in the angular distributions of detached electrons in this geometry with increasing pR, as shown in Fig. 5. The angular distributions provide a clear explanation of

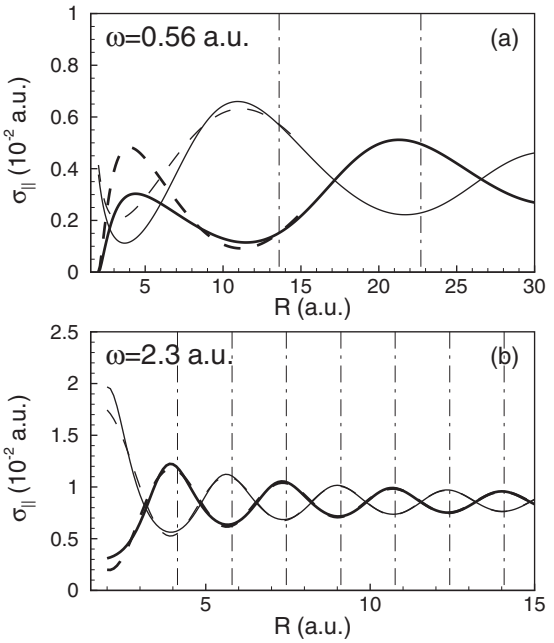

FIG. 4. The dependence of $\sigma_{||}$ on R for $\kappa_1 = \kappa_2 = 1$ a.u. and two different values of ω. Solid thick lines, result (55) for the ground state; solid thin lines, result (55) for the excited state; dashed thick and thin lines, PWA results (58) and (60) for the ground and excited states. Vertical dot-dashed lines mark the approximate positions of the maxima/minima of $\sigma_{||}$ according to Eq. (62).

the origin of the interference fringes. The amplitudes (42b) and (42c) (omitting the beyond-PWA terms proportional to $\tilde{g}_1$), as well as the expression (50), explicitly show that two atomic centers emit two outgoing waves with the phase difference, $\delta = \mathbf{p}\cdot\mathbf{R} = pR\cos\Theta_p$, dependent on p, R, and Θ_p. Thus, the positions of the maxima (minima) in the angular distributions for electrons detached from the ground state are given by Young's formula, $\mathbf{p}\cdot\mathbf{R} = 2\pi n$ [$\mathbf{p}\cdot\mathbf{R} = (2n+1)\pi$]. [For the antisymmetric excited state, these conditions for the positions of the maxima or minima are inverted, as follows from Eq. (59) and as visible in Figs. 3(b) and 3(d)].

To illustrate the interference patterns in axially symmetric (with respect to the direction of the parallel vectors $\mathbf{e}$ and $\mathbf{R}$) angular distributions for parallel geometry and the accuracy of PWA results for this case, in Figs. 6 and 7 we present the results obtained using the exact and the PWA differential cross sections [Eqs. (47) and (48)]. As expected, for large frequencies and R, all side lobes in the angular distributions originate from the double-slit interference of two waves produced by two atomic centers and they are well described in the PWA. However, for frequencies close to the one-photon threshold and/or small R, the PWA results differ considerably from the exact ones (cf. the first columns and first rows in Figs. 6 and 7). Moreover, besides the quantitative differences, additional (not PWA) side lobes appear in the exact results for the angular distributions for $R = 2$ (cf. the results for $pR = 3.39$ in Fig. 6 and for $pR = 1.19$ in Fig. 7). These side lobes clearly indicate the different, not double-slit origin of the interference structures, i.e., the interference between the "PWA" and the "beyond-PWA" pathways of the photodetachment amplitudes, which were discussed below Eq. (46).

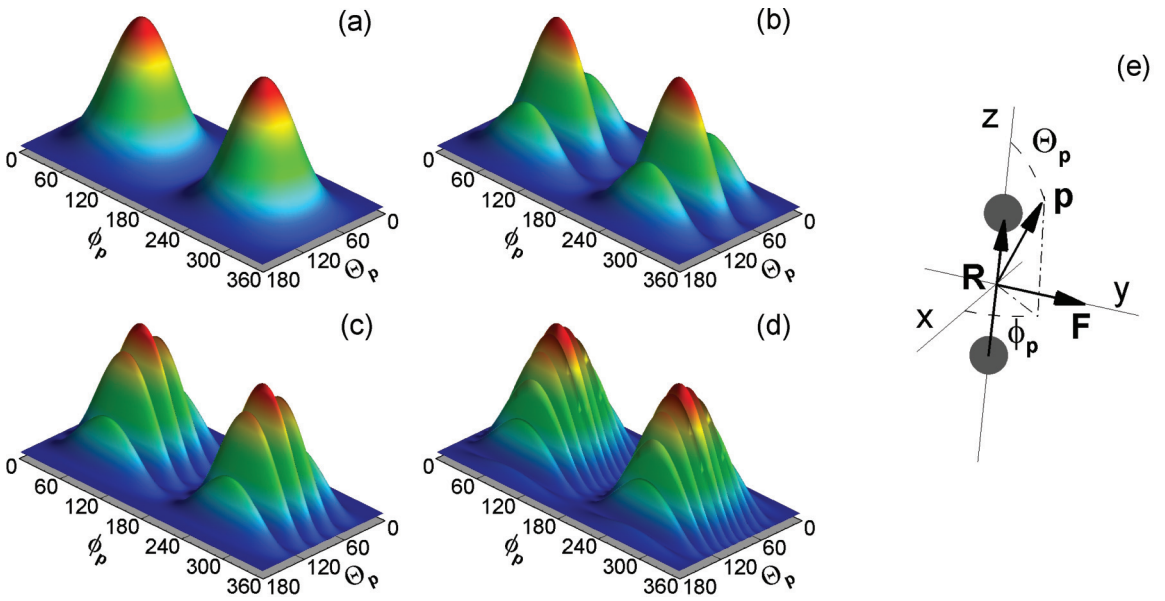

FIG. 5. (Color online) Detached electron angular distributions from the ground state of a molecular system (with $\kappa = 1$ a.u.) for perpendicular geometry and four values of pR: (a) $pR = 2$ a.u.; (b) $pR = 8$ a.u.; (c) $pR = 16$ a.u.; (d) $pR = 32$ a.u. The vectors **R** and **e** are directed along the z axis ($\Theta_p = 0^\circ$) and the y axis ($\Theta_p = 90^\circ$, $\phi_p = 90^\circ$), respectively, where Θ_p and ϕ_p are the polar and azimuthal angles of the detached electron momentum **p** in the reference frame (x, y, z). (e) Sketch of molecular detachment for perpendicular geometry.

3. *Threshold laws for photodetachment cross sections and threshold phenomena in the polarizabilities*

As should be expected, the most striking difference between the exact and the PWA results for the total photodetachment cross sections $\sigma_\pm(\omega, R)$ should appear for $p \to 0$, i.e., in the threshold behavior of $\sigma_\pm$. For the perpendicular geometry, $\sigma_\perp^{(\pm)}$ coincides with $\sigma_\perp^{(\pm,\mathrm{pw})}$; thus, Eq. (60) shows that

$$\sigma_\perp^{(+)} \approx c_{\mathrm{th}}^{(+)}\, p^3, \quad \sigma_\perp^{(-)} \approx \tfrac{1}{10} c_{\mathrm{th}}^{(-)} R^2 p^5, \tag{63}$$

where

$$c_{\mathrm{th}}^{(\pm)} = \frac{64\pi N_\pm}{3ck_\pm^6}. \tag{64}$$

For parallel geometry, mutual cancellations between different terms in $f_{||}^{(\pm,\mathrm{pw})}$ at $pR \to 0$ give $f_{||}^{(+,\mathrm{pw})}|_{pR\to 0} \sim$ const, while $f_{||}^{(-,\mathrm{pw})}|_{pR\to 0} \sim (pR)^2$, which leads to a rapidly

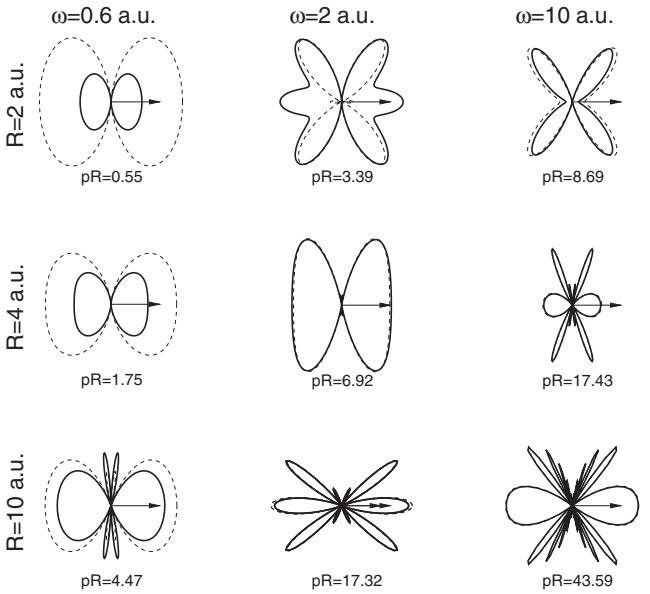

FIG. 6. Angular distributions of electrons detached from the ground state ψ_{E_+} of a two-center system (with $\kappa = 1$ a.u.) for parallel geometry (**e** || **R**) and different R and ω. Arrows show the direction of the vectors **R** and **e**. Solid lines, exact result (47); dashed lines, the PWA result (48).

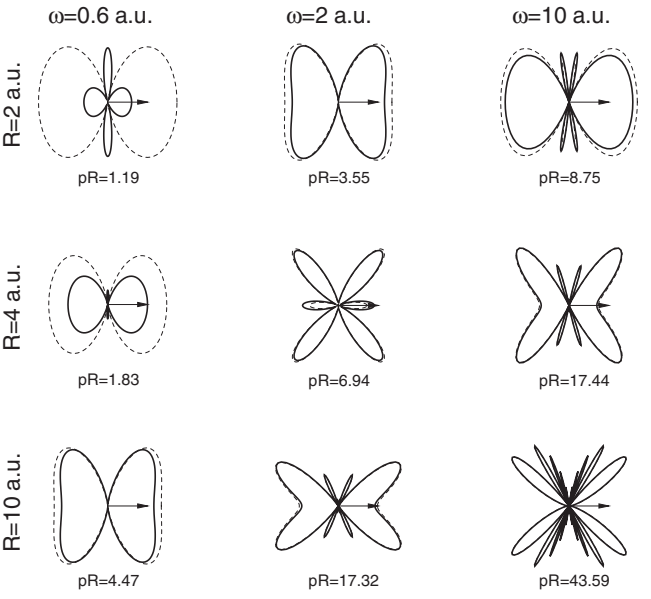

FIG. 7. The same as in Fig. 6 but for the excited state ψ_{E_-}.

decreasing threshold behavior for the excited state, $\sigma_{||}^{(-,\mathrm{pw})}|_{p\to 0} \sim p^5$, while $\sigma_{||}^{(+,\mathrm{pw})}|_{p\to 0} \sim p^3$. However, the exact result for the threshold behavior based on the expression (57) gives

$$\sigma_{||}^{(+)} \approx c_{\mathrm{th}}^{(+)}\left[1+\mathcal{G}_{\mathrm{th}}^{(+)}R^2\left(1+\tfrac{1}{2}\mathcal{G}_{\mathrm{th}}^{(+)}R^2\right)\right]p^3, \tag{65}$$

$$\sigma_{||}^{(-)} \approx 3c_{\mathrm{th}}^{(-)}[\mathcal{G}_{\mathrm{th}}^{(-)}]R^2 p, \tag{66}$$

where

$$\mathcal{G}_{\mathrm{th}}^{(\pm)} = \frac{1}{\kappa R \mp 1}[e^{-k_\pm R}(1+k_\pm R)-1]. \tag{67}$$

For nonequivalent centers, due to lack of permutation symmetry of the wave functions with respect to the atomic centers, the threshold behavior of $\sigma_{||}^{(\pm)}$ [from analysis of $\mathrm{Im}\,\alpha_{||}^{(\pm)}$ in Eq. (33b)] is the same: $\sigma_{||}^{(\pm)}|_{p\to 0} \sim p$ for both states ψ_{E_+} and ψ_{E_-}, while $\sigma_{\perp}^{(+)}|_{p\to 0} \sim p^3$ and $\sigma_{\perp}^{(-)}|_{p\to 0} \sim p^5$ for the perpendicular geometry. Therefore, the exchange interaction significantly affects the threshold behavior of the detachment cross sections for both the ground and the excited states of a two-center system. Note that the above results are compatible with the general analysis of threshold behavior for the total (integrated over θ) photodetachment cross section of diatomic molecular negative ions in Ref. [60] (which does not specify the prefactors multiplying the p dependence of the cross sections).

Branch-point singularities of the polarizabilities $\alpha_{||}^{(\pm)}(\omega,R)$ of the kind $\sqrt{\omega-\omega_{\mathrm{th}}}$ at photodetachment thresholds $\omega_\pm^{\mathrm{th}} = |E_\pm| = k_\pm^2/2$ (originating from the threshold laws for the cross sections $\sigma_{||}^{(\pm)}$) induce known threshold phenomena for the cross section of a process involving a short-range potential (in our case, elastic photon scattering) at the opening of a new reaction channel as the parameters of the problem vary [61,62] (cf. also Ref. [63] on multiphoton detachment from a single δ center). In our case, these threshold phenomena are manifested as "steps" (in which the first derivative in ω does not exist) in the real parts of the polarizabilities at $\omega=\omega_{\mathrm{th}}$. They are visible in inserts in Fig. 3(b) for equivalent centers and in Fig. 8(a) for nonequivalent centers. Note that $\alpha_\kappa^{\mathrm{ZRP}}(\omega)$ has only a higher order branch-point singularity [of the kind $(\omega-\omega_{\mathrm{th}})^{3/2}$], so that $\mathrm{Re}\,\alpha_\kappa^{\mathrm{ZRP}}(\omega)$ in Figs. 2(a) and 2(b) and 3(a) and 3(b) has a point of inflection at $\omega=\omega^{\mathrm{th}}=\kappa^2/2$, in which only the second derivative in ω has a discontinuity.

B. Nonequivalent centers

For nonequivalent centers, an additional parameter, $\rho_\pm$, in Eq. (6) governs the behavior of polarizabilities and detachment cross sections. While for $\rho_\pm \ll 1$ the atomic centers are approximately equivalent ($|c_1^{(\pm)}| \approx |c_2^{(\pm)}|$), the contribution of one of them becomes exponentially suppressed for $\rho_\pm \gg 1$, as discussed below Eq. (8). Hence, results for polarizabilities and total detachment cross sections for $\rho_\pm \gg 1$ are similar to those for a single δ center. In Fig. 8 we present the real part of the polarizability and the total detachment cross section for parallel geometry [the frequency dependencies of $\alpha_\perp^{(\pm)}$ and $\sigma_\perp^{(\pm)}$ are similar to those in Figs. 2(a) and 2(b) and 3(a) and 3(b)]. As for the case of equivalent centers, there is a one-photon resonance; however, its position depends only slightly on

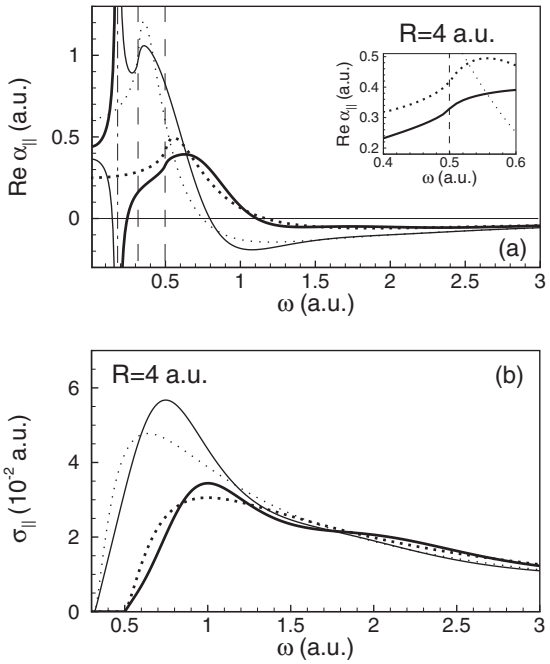

FIG. 8. Frequency dependence of $\alpha_{||}$ and $\sigma_{||}$ for $R=4$ a.u. and $\kappa_1=1$ a.u., $\kappa_2=0.8$ a.u. Thick solid line, ground state ($\rho_+=21.8$); thin solid line, excited state ($\rho_-=9.8$); thick (thin) dotted lines: ZRP result (35) for $j=1$ ($j=2$). Vertical dot-dashed line marks the position of the resonance frequency ω_r. Vertical dashed lines mark the positions of the threshold frequencies $\omega_\pm^{\mathrm{th}}$ ($\omega_+^{\mathrm{th}} \approx 0.5$ a.u. for the ground state; $\omega_-^{\mathrm{th}} \approx 0.32$ a.u. for the exited state).

R since the resonance frequency is well approximated by $\omega_r=(\kappa_1^2-\kappa_2^2)/2$. With increasing R, the resonance features disappear, just as for the case of equivalent centers [cf. Eqs. (51) and (53)].

Two-center interferences in $\mathrm{Re}\,\alpha_{||}^{(\pm)}$ and $\sigma_{||}^{(\pm)}$ are strongly suppressed as compared to the case of equivalent centers due to the large value of the factor $1/\sqrt{1+\rho_\pm^2}$ in Eqs. (33a) and (33b). Thus, the results in Fig. 8 are close to those for a single ZRP. Similarly to Eqs. (60) and (61), the detachment cross section for perpendicular geometry can also be expressed in terms of $\sigma_0^{(\pm)}$ and $f_\perp^{(\pm)}(pR)$,

$$\sigma_\perp^{(\pm)} = \sigma_0^{(\pm)}\left[1+\frac{f_\perp^{(\pm)}(pR)-1}{\sqrt{1+\rho_\pm^2}}\right], \tag{68}$$

while the PWA result for $\sigma_{||}^{(\pm)}$ follows from Eq. (68) by replacing $f_\perp^{(\pm)}$ by $f_{||}^{(\pm,\mathrm{pw})}$ [cf. Eq. (59)].

For perpendicular geometry, the interference patterns in the electron angular distributions for the case of nonequivalent centers rapidly disappear with increasing R due to the damping factor $1/\sqrt{1+\rho_\pm^2}$ in Eq. (50), in which the parameter $\rho_\pm$ exponentially increases with R [cf. Eq. (6)]. In Fig. 9 we present an example of the modification of the angular distributions for the same value of pR, but two different values of R. For small $\rho_\pm$, the shape of the angular distribution is similar to that for equivalent centers [compare Fig. 9(a) with Fig. 5(c)], while in Fig. 9(b) the interference is smeared

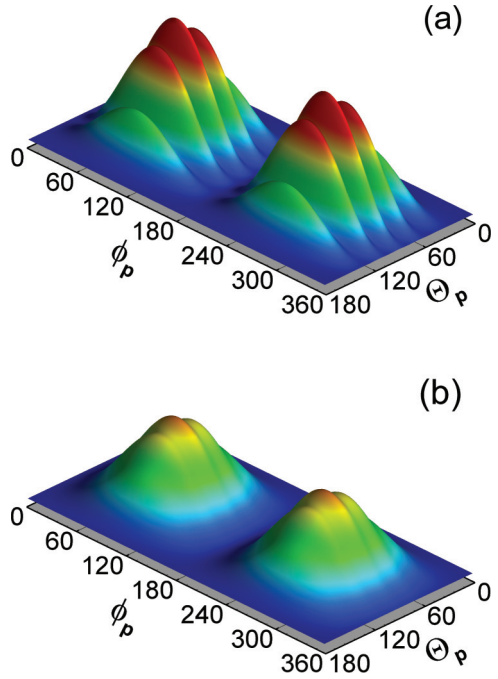

FIG. 9. (Color online) Detached electron angular distributions from the ground state of an asymmetric molecular system ($\kappa_1 = 1$ a.u., $\kappa_2 = 0.8$ a.u.) for perpendicular geometry and the same value of the parameter $pR = 16$ a.u., but different values of R: (a) $R = 2$ a.u., $\rho_+ = 1.53$; (b) $R = 4$ a.u., $\rho_+ = 21.85$. The vectors **R** and **e** are directed along the z axis ($\Theta_p = 0^\circ$) and the y axis ($\Theta_p = 90^\circ$, $\phi_p = 90^\circ$), respectively, where Θ_p and ϕ_p are the polar and azimuthal angles of the detached electron momentum **p** in the reference frame (x,y,z).

out and the angular distribution is similar to that for the single-center case [64]. Recall that even for nonequivalent centers the left-right asymmetry in the angular distributions (with respect to the substitution $\mathbf{p} \to -\mathbf{p}$) is absent for perpendicular geometry. (Note that a similar result was observed in numerical calculations of the differential photoionization cross section for the molecule HeH^{2+} [64].)

1. *Left-right asymmetry in detached electron angular distributions*

For parallel geometry, the crucial difference from the case of equivalent centers consists of breaking the left-right symmetry in the angular distributions, as is seen in Figs. 10 and 11. A number of authors (cf., e.g., Refs. [64–66]) pointed out that the asymmetry cannot be explained within the PWA and that a more accurate treatment of the molecular potential in the continuum state is necessary for its description. Our results also show that the PWA fails to describe even qualitatively the asymmetry of the angular distributions in Figs. 10 and 11.

In our model, the origin of the left-right asymmetry is clear because the symmetry relation (45) for the detachment amplitude $A_1(\mathbf{p})$ is not valid for nonequivalent centers due to the relation (44). That leads to an asymmetry in the angular distributions,

$$\Delta\left(\frac{d\sigma}{d\Omega}\right) \equiv \frac{d\sigma(\mathbf{p})}{d\Omega} - \frac{d\sigma(-\mathbf{p})}{d\Omega}, \tag{69}$$

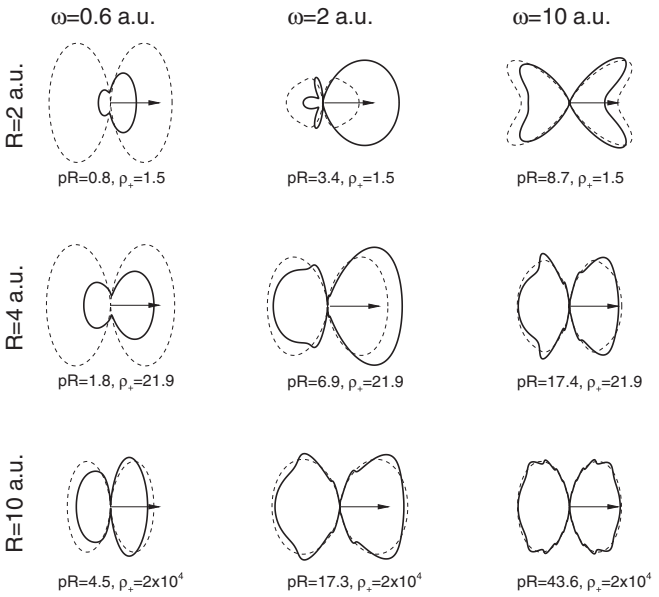

FIG. 10. Left-right asymmetry in detached electron angular distributions from the ground state ψ_{E_+} of a two-center system with nonequivalent centers ($\kappa_1 = 1$ a.u., $\kappa_2 = 0.8$ a.u.) for parallel geometry (**e** || **R**) and different R and ω (cf. Fig. 6). Arrows show the directions of the vectors **R** and **e**. Solid lines, exact result (46); dashed lines, the PWA result (48).

which originates from an interference between the "symmetric" and "antisymmetric" parts of the amplitude $A_1(\mathbf{p})$ (with respect to the substitution $\mathbf{p} \to -\mathbf{p}$).

Equation (46) shows that the contribution of one of the two centers (let us say the second one) to $d\sigma_\pm/d\Omega$ is exponentially small for middle and large distances R due to the exponential smallness of the coefficients $c_2^{(\pm)}$ as compared to $c_1^{(\pm)}$. Thus, for simplicity, we retain only the term with partial amplitude $A_1^{(1)}$ in Eq. (46). [However, we emphasize that this amplitude stores a "memory" of the second center through the factor

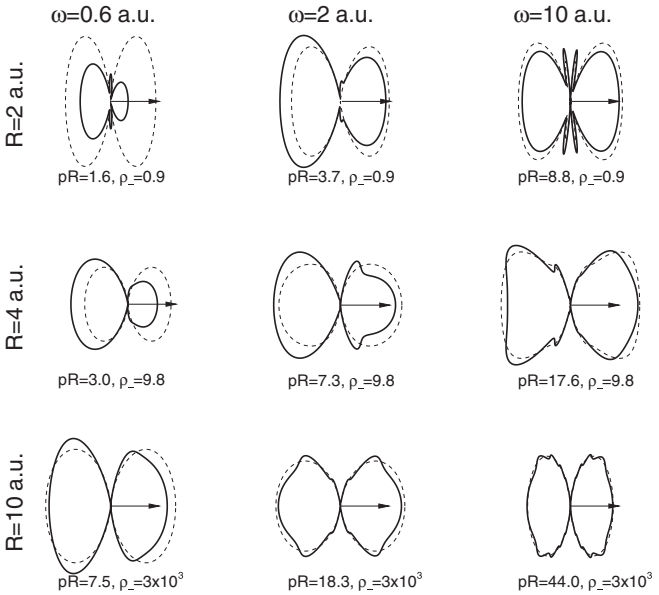

FIG. 11. The same as in Fig. 10 but for the excited state ψ_{E_-}.

$\mathcal{A}_2(-\mathbf{p},\mathbf{p})$ in Eq. (42b).] Moreover, to simplify the explicit form for $\Delta(d\sigma/d\Omega)$, we consider only the major ($\sim R^{-2}$) term in the expansion of $\Delta(d\sigma/d\Omega)$ in series in R^{-1}. As a result, after expansion of $\tilde{g}_1$ and $\mathcal{A}_2(-\mathbf{p},\mathbf{p})$ in Eq. (42b) in R^{-1}, we obtain

$$\Delta\left(\frac{d\sigma}{d\Omega}\right) = \frac{4p^2\kappa_1}{c\omega^3}\frac{(\mathbf{e}\cdot\mathbf{p})(\mathbf{e}\cdot\mathbf{R})}{R^2\sqrt{\kappa_2^2+p^2}}\cos(pR+\delta_2)\cos(\mathbf{p}\cdot\mathbf{R}), \tag{70}$$

where $\tan\delta_2 = -p/\kappa_2$, so that δ_2 is the s-wave scattering phase for the second δ center (which is the only nonzero scattering phase for a single-center ZRP model [32]). Note that the factor $1/\sqrt{\kappa_2^2+p^2}$ in Eq. (70) is the modulus of the isotropic electron scattering amplitude for a ZRP, $f_{\kappa_2}(p) = 1/(\kappa_2 + ip)$ [32], to which the modulus of $\mathcal{A}_2(-\mathbf{p},\mathbf{p})$ reduces for large R. [In Eq. (70) we give the result for the ground state, while the result for the excited state can be obtained from Eq. (70) by changing the overall sign and making the replacements: $\kappa_1 \to \kappa_2$, $\kappa_2 \to \kappa_1$, $\delta_2 \to \delta_1$.]

The result (70) provides a transparent physical explanation for the interference origin of the asymmetric angular distributions. After absorption of a photon by the electron localized near the first center, one part of the electron wave function (the plane-wave part) reaches the detector directly while the other part scatters from the second δ center, accumulating a phase difference $pR+\delta_2$ (where pR is the "geometrical" phase and δ_2 is the quantum mechanical scattering phase). Thus, the second center produces a secondary (scattered) wave (cf. Fig. 12). The geometrical phase difference between the secondary and initial ("direct") waves leads to an interference factor $\cos(\mathbf{p}\cdot\mathbf{R})$ in Eq. (70). This is a direct analog of the interference patterns observed in heteronuclear diatomic molecules [59,67,68]. In complex systems, similar interference patterns in photoionization of well-localized core electrons due to scattering from adjacent atoms form the basis of extended x-ray absorption fine structure (EXAFS) spectroscopy [69].

Integrating Eq. (70) over the electron momentum angles in the right hemisphere, we obtain (to lowest order in R^{-1})

$$\Delta\sigma = \frac{8\pi p^2\kappa_1}{\omega^3 c}\frac{(\mathbf{e}\cdot\mathbf{R})^2}{R^4\sqrt{\kappa_2^2+p^2}}\cos(pR+\delta_2)\sin(pR). \tag{71}$$

Analysis of Eq. (71) shows that for $p > \kappa_+$ and $R > \kappa_-^{-1}$, $\Delta\sigma$ takes negative values only over small intervals of pR. Thus, the angular distribution is mostly localized on the side of the atomic center with larger κ (i.e., κ_1), in agreement with numerical results in Fig. 10. The general shapes of the angular distributions for detachment from the excited state are inverted from those for the ground state (cf. Fig. 11).

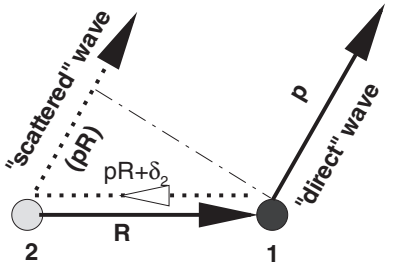

FIG. 12. Sketch of two pathways for one-photon detachment.

VII. SUMMARY AND CONCLUSIONS

In summary, we have presented a general analysis for a two-center δ potential model of a one-electron diatomic molecular ion system interacting with an intense, monochromatic laser field. Our results generalize the results for a single-center ZRP model [46], obtained for an arbitrarily polarized, intense laser field, to the case of two δ centers. The ultimate goal of this work is to obtain closed-form analytic expressions for the rates for strong-field molecular processes involving this simple model system. Such closed-form analytic formulas will provide analytical insight into the dependence of these rates on key laser and molecular parameters.

In this paper we have focused on the development of a general formulation of the strong-field molecular problem and on the application of this formulation in the weak-field limit. In the weak-field limit we have analyzed the frequency-dependent polarizability and the photodetachment cross section for the molecular ion model system. We have examined these molecular properties for both homonuclear and heteronuclear cases and for various values of the key laser and molecular parameters of the problem. Where possible, we have delineated the connection to analyses of other authors concerning both interference effects on detached electron angular distributions and the validity of the PWA for describing the detached electron. We have also analyzed the low-frequency limit of our results in order to present results for a static electric field.

From the weak-field results we have obtained, we conclude that the simple molecular model we have analyzed does provide results that reflect the essential physics of the problem and its dependence on key laser and molecular parameters. Knowledge of the weak-field limit results we have presented in this paper will be essential in order to determine if the rates for strong-field molecular processes, such as for HHG, can be factorized. Analysis of the rates for such strong-field processes will be presented elsewhere.

ACKNOWLEDGMENTS

This work was supported in part by RFBR Grants No. 12-02-12101-ofi_m and No. 13-02-00447-a, by NSF Grant No. PHY-1208059, by the Russian Federation Ministry of Education and Science (Contract No. 14.B37.21.1937), and by the "Dynasty" Foundation (M.V.F.). M. Yu. Ivanov acknowledges the warm hospitality of the Voronezh State University, where the major part of this work has been performed within the framework of the collaborative program funded by the Russian Federation Ministry of Education and Science.

APPENDIX A: MATRIX FORM OF THE INTEGRAL EQUATIONS (24)

To convert Eqs. (24) to an infinite system of linear equations for the Fourier coefficients $\hat{f}_k^{(j)}$ of $\hat{f}_j(t)$, we expand both the right and left sides of Eqs. (24) in Fourier series and equate coefficients for the same harmonics. In what follows, we

present the matrix form of these equations for the cases of linear and circular polarization of the field $\mathbf{F}(t)$.

1. The case of linear polarization: $\mathbf{F}(t) = \mathbf{F}\cos\omega t$

Using the above-described procedure, for the case of linear polarization we obtain the following pair of coupled matrix equations for the Fourier expansion coefficients:

$$\begin{aligned}(i\sqrt{2\hat{\epsilon}_{k,k}}+\kappa_1)\hat{f}_k^{(1)} + R^{-1}e^{i\sqrt{2\hat{\epsilon}_{k,k}}R}\hat{f}_k^{(2)} &= \sum_{k'}\left[\hat{M}_{k,k'}\hat{f}_{k'}^{(1)} + \hat{N}_{k,k'}(\mathbf{R})\hat{f}_{k'}^{(2)}\right],\\ R^{-1}e^{i\sqrt{2\hat{\epsilon}_{k,k}}R}\hat{f}_k^{(1)} + (i\sqrt{2\hat{\epsilon}_{k,k}}+\kappa_2)\hat{f}_k^{(2)} &= \sum_{k'}\left[\hat{N}_{k,k'}(-\mathbf{R})\hat{f}_{k'}^{(1)} + \hat{M}_{k,k'}\hat{f}_{k'}^{(2)}\right],\end{aligned} \tag{A1}$$

where the matrix elements $\hat{N}_{k,k'}$ can be presented in integral form,

$$\hat{N}_{k,k'}(\mathbf{R}) = -\frac{(-1)^{k-k'}}{\sqrt{2\pi i}}\int_0^\infty \frac{d\tau}{\tau^{3/2}}e^{i\hat{\epsilon}_{k,k'}\tau + i\frac{R^2}{2\tau}} \times [e^{i\lambda(\tau)}\mathcal{J}_{k-k'}[\lambda(\tau),\beta(\tau)] - \delta_{k,k'}], \tag{A2}$$

where $\mathcal{J}_{k-k'}$ is the generalized Bessel function,

$$\mathcal{J}_{k-k'}(\lambda,\beta) = \sum_s i^{-s}J_s(\lambda)J_{k-k'+2s}(\beta), \tag{A3}$$

and where we have introduced the notations,

$$\hat{\epsilon}_{k,k'} = \hat{\epsilon} + \frac{k+k'}{2}\omega, \tag{A4a}$$

$$\lambda(\tau) = \frac{4u_p}{\omega}\frac{\sin^2(\omega\tau/2)}{\omega\tau}, \tag{A4b}$$

$$\beta(\tau) = \frac{\mathbf{F}\cdot\mathbf{R}}{\omega}\frac{\sin(\omega\tau/2)}{\omega\tau/2}. \tag{A4c}$$

The matrix elements $\hat{M}_{k',k}$ equal zero for odd $k-k' = 2s+1$, while for even $k-k' = 2s$, they are given by

$$\hat{M}_{k-2s,k} = -\frac{i^s}{\sqrt{2\pi i}}\int_0^\infty \frac{d\tau}{\tau^{3/2}}e^{i\hat{\epsilon}_{k,k-2s}\tau} \times\{e^{i\lambda(\tau)}J_s[\lambda(\tau)] - \delta_{k,k-2s}\}. \tag{A5}$$

The explicit forms of the matrix elements (A2) and (A5) allow one to verify the important symmetry relations,

$$\hat{M}_{k,k'} = \hat{M}_{k',k}, \quad \hat{N}_{k,k'}(\mathbf{R}) = \hat{N}_{k',k}(-\mathbf{R}), \tag{A6}$$

where the first relation follows from the properties of the Bessel function,

$$J_{-s}(x) = (-1)^s J_s(x),$$

while the second one follows from the relation,

$$\mathcal{J}_{k-k'}(\lambda,\beta) = \mathcal{J}_{k'-k}(\lambda,-\beta).$$

It follows from the symmetry relations (A6) that the matrix in Eq. (A1) can be presented in a symmetric form, so that it can be diagonalized. Thus, the system (A1) of *homogeneous* equations has nontrivial solutions for those complex quasienergies $\hat{\epsilon}$, for which one of the matrix elements of the diagonalized system (A1) vanishes. The corresponding Fourier coefficients $\hat{f}_k^{(j)}$ can be found as the components of the eigenvectors for a given $\hat{\epsilon}$.

Note that matrix elements $\hat{M}_{k',k}$ do not depend on the internuclear distance R, which enters only into the exchange-interaction-induced matrix elements $\hat{N}_{k,k'}$. Since the latter vanish in the limit $R\to\infty$ [as do the R-dependent factors on the left sides of Eqs. (A1)], the system (A1) in this limit reduces to two independent subsystems for the complex quasienergies and Fourier coefficients of functions $\hat{f}_j(t)$ for two isolated δ centers [46].

2. The case of circular polarization: $\mathbf{F}(t) = \frac{F}{\sqrt{2}}(\mathbf{e}_x\cos\omega t + \eta\mathbf{e}_y\sin\omega t)$, $\eta = \pm 1$

Since the function $f(t)$ for an electron in a single δ center becomes independent of the time t for the case of a circularly polarized field [36,37], the matrix form of Eq. (24) for this case simplifies significantly as compared to Eq. (A1) and may be presented in the form

$$\begin{aligned}(i\sqrt{2\hat{\epsilon}_{k,k}}+\kappa_1+\hat{\mathcal{M}}_{k,k})\hat{f}_k^{(1)} + R^{-1}e^{i\sqrt{2\hat{\epsilon}_{k,k}}R}\hat{f}_k^{(2)} &= \sum_{k'}\hat{\mathcal{N}}_{k,k'}(\mathbf{R})\hat{f}_{k'}^{(2)},\\ R^{-1}e^{i\sqrt{2\hat{\epsilon}_{k,k}}R}\hat{f}_k^{(1)} + (i\sqrt{2\hat{\epsilon}_{k,k}}+\kappa_2+\hat{\mathcal{M}}_{k,k})\hat{f}_k^{(2)} &= \sum_{k'}\hat{\mathcal{N}}_{k,k'}(-\mathbf{R})\hat{f}_{k'}^{(1)},\end{aligned} \tag{A7}$$

where

$$\hat{\mathcal{M}}_{k,k} = \frac{1}{\sqrt{2\pi i}}\int_0^\infty \frac{d\tau}{\tau^{3/2}}e^{i\hat{\epsilon}_{k,k}\tau}[e^{i\lambda(\tau)}-1], \tag{A8}$$

$$\hat{\mathcal{N}}_{k,k'} = -\frac{1}{\sqrt{2\pi i}}\int_0^\infty \frac{d\tau}{\tau^{3/2}}e^{i\hat{\epsilon}_{k,k'}\tau + i\frac{R^2}{2\tau}} \times\{e^{i\lambda(\tau)}J_{k'-k}[\hat{\beta}(\tau)] - \delta_{k,k'}\}, \tag{A9}$$

$$\hat{\beta}(\tau) = \frac{FR\cos\Xi}{\sqrt{2}\omega}\frac{\sin(\omega\tau/2)}{\omega\tau/2}, \tag{A10}$$

and where Ξ is the angle between the vector $\mathbf{R}$ and the polarization plane of the laser field.

We have confirmed that the system of exact eigenvalue equations (A7) for the complex quasienergies of an electron in the ZRP molecular model is equivalent to that obtained in Ref. [35] using different mathematical techniques for the treatment of the QQES equations.

APPENDIX B: DERIVATIONS OF EQS. (31)–(33b)

The general form (31) for the complex quasienergy $\epsilon_\pm$ in the lowest nonvanishing order in the amplitude F of a monochromatic field $\mathbf{F}\cos\omega t$ follows from general arguments, as well as from a perturbative (in F) analysis of the exact matrix equation (A1). To obtain explicit expressions for the polarizability $\alpha_\pm$, we analyze the matrix elements in the system (A1) in the limit $F\to 0$. This analysis shows that only Fourier coefficients $\hat{f}_k^{(j)}$ with $|k| = 1$ are induced by the laser field in the lowest (first) order of PT in F. The explicit form of these coefficients can be found from the system of Eqs. (A1) by considering the right-hand side (rhs) in these equations as a perturbation. Substituting in the rhs of Eq. (A1) the coefficients

$\hat{f}_{k'}^{(j)}$ in the form $\hat{f}_{k'}^{(j)} = \hat{f}_0^{(j)}\delta_{k',0}$ and taking into account that $\hat{M}_{\pm1,0} = 0$ [cf. Eq. (A5)], we obtain

$$\begin{pmatrix} ip_k + \kappa_1 & \frac{e^{ip_k R}}{R} \\ \frac{e^{ip_k R}}{R} & ip_k + \kappa_2 \end{pmatrix} \begin{pmatrix} \hat{f}_k^{(1)} \\ \hat{f}_k^{(2)} \end{pmatrix} = \begin{pmatrix} \hat{N}_{k,0}(\mathbf{R})\hat{f}_0^{(2)} \\ \hat{N}_{0,k}(\mathbf{R})\hat{f}_0^{(1)} \end{pmatrix}, \quad \text{(B1)}$$

where $p_k \equiv \sqrt{2\hat{\epsilon}_{k,k}} = \sqrt{2(\hat{\epsilon} + k\omega)}$. The matrix elements $\hat{N}_{k,0}$ to first order in F (but with the exact quasienergy $\hat{\epsilon}$) are

$$\hat{N}_{k,0}(\mathbf{R}) = -\hat{N}_{0,k}(\mathbf{R}) = -\frac{FR\cos\theta}{2\omega^2} g_k, \quad \text{(B2)}$$

$$g_k \equiv g_k(R,\hat{\epsilon},\omega) = \frac{1}{R}\frac{\partial}{\partial R}\frac{e^{ip_k R} - e^{i\sqrt{2\hat{\epsilon}}}}{R}. \quad \text{(B3)}$$

The solution of Eq. (B1) for $\hat{f}_k^{(1)}$ and $\hat{f}_k^{(2)}$ in terms of the coefficients $\hat{f}_0^{(j)}$ is given by

$$\hat{f}_k^{(1)} = -\frac{FR\cos\theta g_k}{2\omega^2\Delta(p_k)}\left[\frac{e^{ip_k R}}{R}\hat{f}_0^{(1)} + (\kappa_2 + ip_k)\hat{f}_0^{(2)}\right], \quad \text{(B4a)}$$

$$\hat{f}_k^{(2)} = \frac{FR\cos\theta g_k}{2\omega^2\Delta(p_k)}\left[\frac{e^{ip_k R}}{R}\hat{f}_0^{(2)} + (\kappa_1 + ip_k)\hat{f}_0^{(1)}\right], \quad \text{(B4b)}$$

where the definition for $\Delta(p_k)$ is given by Eq. (10).

Two equations of the system (A1) for $k = 0$, in which only terms with $k' = -1,0,1$ are taken into account and the explicit form (B4) for the coefficients $\hat{f}_{\pm1}^{(1)}$ and $\hat{f}_{\pm1}^{(2)}$ is used, compose a homogeneous system of equations for the coefficients $\hat{f}_0^{(j)}$ and the quasienergy $\hat{\epsilon}$,

$$\begin{pmatrix} \mathcal{M}_{0,0}^{(1)} & \mathcal{N}_{0,0} \\ \mathcal{N}_{0,0} & \mathcal{M}_{0,0}^{(2)} \end{pmatrix} \begin{pmatrix} \hat{f}_0^{(1)} \\ \hat{f}_0^{(2)} \end{pmatrix} = 0, \quad \text{(B5)}$$

where

$$\mathcal{M}_{0,0}^{(j)} = i\sqrt{2\hat{\epsilon}} + \kappa_j - \hat{M}_{00} - \sum_{k'=\pm1} \hat{N}_{0,k'}^2(\mathbf{R})\frac{\kappa_j + ip_{k'}}{\Delta(p_{k'})},$$

$$\mathcal{N}_{0,0} = \frac{e^{i\sqrt{2\hat{\epsilon}}R}}{R} - \hat{N}_{0,0} - \sum_{k'=\pm1} \hat{N}_{0,k'}^2(\mathbf{R})\frac{e^{ip_{k'}R}}{R\Delta(p_{k'})}, \quad \text{(B6)}$$

and the lowest (second)-order in F expansions of the matrix elements $\hat{M}_{0,0}$ and $\hat{N}_{00}$ have the form

$$\hat{M}_{0,0} = -\frac{F^2}{12\omega^4}[(2\omega - 2\hat{\epsilon})^{3/2} - 2(-2\hat{\epsilon})^{3/2} + i(2\omega + 2\hat{\epsilon})^{3/2}],$$

$$\hat{N}_{0,0} = -\frac{F^2}{4\omega^4}\left(1 + R\cos^2\theta\frac{\partial}{\partial R}\right)(\tilde{g}_1 + \tilde{g}_{-1}), \quad \text{(B7)}$$

where the factors $\tilde{g}_{\pm1}$ are given by Eq. (34).

Nontrivial solutions of the homogeneous system (B5) exist for those quasienergies $\hat{\epsilon}$ (or $\epsilon = \hat{\epsilon} - u_p$) that satisfy a transcendental equation,

$$\mathcal{M}_{0,0}^{(1)}\mathcal{M}_{0,0}^{(2)} - \mathcal{N}_{0,0}^2 = 0, \quad \text{(B8)}$$

which also can be represented in an alternative form as a set of two independent equations [cf. Eqs. (4) and (5)]:

$$\frac{\mathcal{M}_{0,0}^{(1)} + \mathcal{M}_{0,0}^{(2)}}{2} = \mp\sqrt{\left(\frac{\mathcal{M}_{0,0}^{(1)} - \mathcal{M}_{0,0}^{(2)}}{2}\right)^2 + \mathcal{N}_{0,0}^2}. \quad \text{(B9)}$$

Substituting the expansion (31) for ϵ in Eq. (B6) for the matrix elements $\mathcal{M}_{0,0}^{(j)}$ and $\mathcal{N}_{0,0}$ (involving $\hat{\epsilon} = \epsilon - u_p$), expanding then both sides of Eq. (B9) in series in F up to terms of order $\sim F^2$ and then equating coefficients multiplying the same powers of F, we obtain the parametrization (32) for $\alpha_\pm$ in Eq. (31) and explicit expressions (33a) and (33b) for the perpendicular and parallel polarizabilities.

[1] A. Giusti-Suzor, X. He, O. Atabek, and F. H. Mies, Phys. Rev. Lett. **64**, 515 (1990).
[2] P. H. Bucksbaum, A. Zavriyev, H. G. Muller, and D. W. Schumacher, Phys. Rev. Lett. **64**, 1883 (1990).
[3] K. Codling, L. J. Frasinski, and P. A. Hatherly, J. Phys. B **22**, L321 (1989).
[4] T. Seideman, M. Y. Ivanov, and P. B. Corkum, Phys. Rev. Lett. **75**, 2819 (1995).
[5] T. Zuo and A. D. Bandrauk, Phys. Rev. A **52**, R2511 (1995).
[6] E. Constant, H. Stapelfeldt, and P. B. Corkum, Phys. Rev. Lett. **76**, 4140 (1996).
[7] I. V. Litvinyuk, K. F. Lee, P. W. Dooley, D. M. Rayner, D. M. Villeneuve, and P. B. Corkum, Phys. Rev. Lett. **90**, 233003 (2003).
[8] A. Jaroń-Becker, A. Becker, and F. H. M. Faisal, Phys. Rev. A **69**, 023410 (2004).
[9] M. Abu-samha and L. B. Madsen, Phys. Rev. A **81**, 033416 (2010).
[10] X. M. Tong, Z. X. Zhao, and C. D. Lin, Phys. Rev. A **66**, 033402 (2002).
[11] K.-J. Yuan and A. D. Bandrauk, Phys. Rev. A **84**, 013426 (2011).
[12] J. Itatani, J. Levesque, D. Zeidler, H. Niikura, H. Pépin, J. C. Kieffer, P. B. Corkum, and D. M. Villeneuve, Nature (London) **432**, 867 (2004).
[13] A.-T. Le, R. R. Lucchese, S. Tonzani, T. Morishita, and C. D. Lin, Phys. Rev. A **80**, 013401 (2009).
[14] M. Y. Ivanov, T. Brabec, and N. Burnett, Phys. Rev. A **54**, 742 (1996).
[15] M. Okunishi, H. Niikura, R. R. Lucchese, T. Morishita, and K. Ueda, Phys. Rev. Lett. **106**, 063001 (2011).
[16] C. I. Blaga, J. Xu, A. D. DiChiara, E. S. K. Zhang, P. Agostini, T. A. Miller, L. F. DiMauro, and C. D. Lin, Nature (London) **483**, 194 (2012).
[17] K.-J. Yuan, H. Z. Lu, and A. D. Bandrauk, Phys. Rev. A **80**, 061403(R) (2009).
[18] M. V. Frolov, N. L. Manakov, E. A. Pronin, and A. F. Starace, Phys. Rev. Lett. **91**, 053003 (2003).
[19] M. V. Frolov, N. L. Manakov, and A. F. Starace, Phys. Rev. A **78**, 063418 (2008).
[20] M. V. Frolov, N. L. Manakov, T. S. Sarantseva, and A. F. Starace, J. Phys. B **42**, 035601 (2009).

[21] M. V. Frolov, N. L. Manakov, T. S. Sarantseva, and A. F. Starace, Phys. Rev. A **83**, 043416 (2011).
[22] M. V. Frolov, N. L. Manakov, T. S. Sarantseva, M. Yu. Emelin, M. Yu. Ryabikin, and A. F. Starace, Phys. Rev. Lett. **102**, 243901 (2009).
[23] M. V. Frolov, N. L. Manakov, and A. F. Starace, Phys. Rev. A **79**, 033406 (2009).
[24] A. V. Flegel, M. V. Frolov, N. L. Manakov, and A. N. Zheltukhin, J. Phys. B **42**, 241002 (2009).
[25] A. V. Flegel, M. V. Frolov, N. L. Manakov, A. F. Starace, and A. N. Zheltukhin, Phys. Rev. A **87**, 013404 (2013).
[26] M. V. Frolov, N. L. Manakov, A. A. Silaev, N. V. Vvedenskii, and A. F. Starace, Phys. Rev. A **83**, 021405 (2011).
[27] M. V. Frolov, N. L. Manakov, A. M. Popov, O. V. Tikhonova, E. A. Volkova, A. A. Silaev, N. V. Vvedenskii, and A. F. Starace, Phys. Rev. A **85**, 033416 (2012).
[28] M. V. Frolov, D. V. Knyazeva, N. L. Manakov, A. M. Popov, O. V. Tikhonova, E. A. Volkova, M.-H. Xu, L.-Y. Peng, L.-W. Pi, and A. F. Starace, Phys. Rev. Lett. **108**, 213002 (2012).
[29] M. V. Frolov, N. L. Manakov, T. S. Sarantseva, and A. F. Starace, Phys. Rev. A **86**, 063406 (2012).
[30] A. N. Zheltukhin, N. L. Manakov, A. V. Flegel, and M. V. Frolov, Zh. Eksp. Teor. Fiz. Pis. Red. **84**, 641 (2011) [JETP Lett. **94**, 599 (2011)].
[31] B. M. Smirnov and O. B. Firsov, Zh. Eksp. Teor. Fiz. **47**, 232 (1964) [Sov. Phys. JETP **20**, 156 (1965)].
[32] Y. N. Demkov and V. N. Ostrovsky, *Zero-Range Potentials and Their Applications in Atomic Physics* (Plenum, New York, 1988).
[33] F. Dalidchik and V. Slonim, Zh. Eksp. Teor. Fiz. **70**, 47 (1976) [Sov. Phys. JETP **43**, 25 (1976)].
[34] S. V. Borzunov, N. L. Manakov, A. F. Starace, and M. V. Frolov, Zh. Eksp. Teor. Fiz. **139**, 835 (2011) [Sov. Phys. JETP **112**, 725 (2011)].
[35] P. S. Krstić, D. B. Milošević, and R. K. Janev, Phys. Rev. A **44**, 3089 (1991).
[36] N. L. Manakov and L. P. Rapoport, Zh. Eksp. Teor. Fiz. **69**, 842 (1975) [Sov. Phys. JETP **42**, 430 (1976)].
[37] I. J. Berson, J. Phys. B **8**, 3078 (1975).
[38] R. Kopold, W. Becker, and M. Kleber, Phys. Rev. A **58**, 4022 (1998).
[39] A. Afaq and M. L. Du, Commun. Theor. Phys. **46**, 119 (2006).
[40] A. Afaq and M. L. Du, Commun. Theor. Phys. **50**, 1401 (2008).
[41] A. Afaq and M. L. Du, J. Phys. B **42**, 105101 (2009).
[42] D.-H. Wang, Chin. Phys. B **19**, 020306 (2010).
[43] D.-H. Wang, T. Tang, and S. Wang, Mol. Phys. **108**, 1385 (2010).
[44] T. K. Rebane and R. I. Sharibzhanov, Teor. Eksp. Khim. **13**, 381 (1977) [Theor. Exp. Chem. **13**, 286 (1977)].
[45] N. L. Manakov, V. D. Ovsiannikov, and L. P. Rapoport, Phys. Rep. **141**, 319 (1986).
[46] N. L. Manakov and A. G. Fainshtein, Zh. Eksp. Teor. Fiz. **79**, 751 (1980) [Sov. Phys. JETP **52**, 382 (1980)].
[47] N. L. Manakov, M. V. Frolov, B. Borca, and A. F. Starace, J. Phys. B **36**, R49 (2003).
[48] D. I. Bondar, R. Murray, and M. Yu. Ivanov, arXiv:0907.2044.
[49] F. Dalidchik and V. Slonim, Teor. Eksp. Khim. **13**, 3 (1977) [Theor. Exp. Chem. **13**, 1 (1977)].
[50] N. L. Manakov, M. A. Preobrazhenskii, L. P. Rapoport, and A. G. Fainshtein, Zh. Eksp. Teor. Fiz. **75**, 1243 (1978) [Sov. Phys. JETP **48**, 626 (1978)].
[51] Note that an overall factor 1/2 was inadvertently omitted in Eq. (48) of Ref. [34].
[52] B. A. Zon and E. I. Sholokhov, Zh. Eksp. Teor. Fiz. **70**, 887 (1976) [Sov. Phys. JETP **43**, 461 (1976)].
[53] N. L. Manakov, V. D. Ovsyannikov, and L. P. Rapoport, Zh. Eksp. Teor. Fiz. **70**, 1697 (1976) [Sov. Phys. JETP **43**, 885 (1976)].
[54] V. B. Berestetskii, E. M. Lifshitz, and L. P. Pitaevskii, *Quantum Electrodynamics* (Pergamon, Oxford, 1982).
[55] X. Guan, E. B. Secor, K. Bartschat, and B. I. Schneider, Phys. Rev. A **84**, 033420 (2011).
[56] A. G. Fainshtein, N. L. Manakov, V. D. Ovsiannikov, and L. P. Rapoport, Phys. Rep. **210**, 111 (1992).
[57] H. D. Cohen and U. Fano, Phys. Rev. **150**, 30 (1966).
[58] I. G. Kaplan and A. P. Markin, Dok. Akad. Nauk SSSR **184**, 66 (1969) [Sov. Phys. Dokl. **14**, 36 (1969)].
[59] S. E. Canton, E. Plésiat, J. D. Bozek, B. S. Rude, P. Decleva, and F. Martín, Proc. Natl. Acad. Sci. USA **108**, 7302 (2011).
[60] S. Geltman, Phys. Rev. **112**, 176 (1958).
[61] A. I. Baz', Zh. Eksp. Teor. Fiz. **33**, 923 (1957) [Sov. Phys. JETP **6**, 709 (1958)].
[62] A. I. Baz', Y. B. Zeldovich, and A. M. Perelomov, *Scattering, Reactions and Decays in Nonrelativistic Quantum Mechanics*, 2nd ed. (Nauka, Moscow, 1971).
[63] B. Borca, M. V. Frolov, N. L. Manakov, and A. F. Starace, Phys. Rev. Lett. **88**, 193001 (2002).
[64] X. Guan, E. B. Secor, R. C. DuToit, and K. Bartschat, Phys. Rev. A **86**, 053425 (2012).
[65] G. L. Yudin, S. Patchkovskii, and A. D. Bandrauk, J. Phys. B **39**, 1537 (2006).
[66] H. Miyagi, T. Morishita, and S. Watanabe, Phys. Rev. A **85**, 022708 (2012).
[67] B. Zimmermann, D. Rolles, B. Langer, R. Hentges, M. Braune, S. Cvejanovic, O. Geßner, F. Heiser, S. Korica, T. Lischke *et al.*, Nat. Phys. **4**, 649 (2008).
[68] U. Becker, Nature (London) **474**, 586 (2011).
[69] B. K. Teo, *EXAFS: Basic Principles and Data Analysis* (Springer, Verlag, 1986).